



Technische Universität München
TUM School of Engineering and Design
Photogrammetrie und Fernerkundung
Prof. Dr.-Ing. U. Stilla

Evaluation of the Effect of Enriched Facade Models on Image-Based Localization of Vehicles

Antonia Bieringer

Bachelor's Thesis

Submission: 01.04.2023 - 02.09.2023

Study Course: Geodesy and Geoinformation (Bachelor)


Supervisors: M.Sc. Olaf Wysocki
Dr.-Ing. Sebastian Tuttas
Prof. Dr.-Ing. habil. Ludwig Hoegner

In Cooperation with:



I confirm that this Bachelor's Thesis is my own work and I have documented all sources and material used.

Munich, 22.08.2023


Antonia Bieringer

Abstract

Numerous navigation applications rely on data from global navigation satellite systems (GNSS), even though their accuracy is compromised in urban areas, posing a significant challenge, particularly for precise autonomous car localization.

Extensive research has focused on enhancing outcomes by integrating various sensor types to address this. This thesis introduces a novel approach for car localization, leveraging image features that correspond with highly detailed semantic 3D building models.

The core concept involves augmenting accuracy by incorporating prior environmental knowledge into calculations. The study assesses outcomes using Level-of-Detail 2 (LoD2) and Level-of-Detail 3 (LoD3) models, examining whether models enriched with facades yield superior accuracy. This examination encompasses diverse methods, including off-the-shelf feature matching and machine learning, facilitating comprehensive analysis and discussion.

The results of the thesis have an impact for the field of navigation in areas where GNSS is not available.

Contents

Abstract	ii
1. Introduction	1
1.1. Motivation	1
1.2. Challenges	1
1.3. Thesis Outline	2
2. State of the Art	3
2.1. Localization Methods Based on Relative Positioning	3
2.1.1. Inertial Navigation	3
2.2. Localization Method Based on Satellites	4
2.3. Localization Methods Based on Images	5
2.3.1. Algorithms for Feature Detection	5
2.3.2. Algorithms for Localizing and Mapping	8
2.4. Localization Methods Based on LoD2 Models	9
3. Methodology	10
3.1. Overview of the Final Workflow	10
3.2. Creating Virtual Images of the LoD3 Model	11
3.3. Feature Matching	13
3.4. Correlating the Features with a 3D-Coordinate	15
3.5. Calculating the Trajectory	15
4. Experiments	17
4.1. Dataset	17
4.2. Different Approaches for Feature Matching	18
4.2.1. Corresponding Image-Pairs of Different Types	19
4.2.2. Segmented Images with Machine Learning	19
4.2.3. Sobel-Filter and Canny Edge Detection	20
4.3. Results	22
4.3.1. Number of Features	22
4.3.2. Deviation from the Trajectory	23
4.3.3. Accuracies of the Calculated Camera Position	25

Contents

5. Discussion	28
5.1. Evaluation of the Developed Methodology	28
5.2. Evaluation of the Achieved Accuracies	29
5.3. Comparison with GNSS Data	31
6. Conclusions and Outlook	32
6.1. Key Findings	32
6.2. Real-World Applications and Implications	32
6.3. Future Research Directions	33
List of Figures	34
List of Tables	35
Bibliography	36
A. Appendix	38

1. Introduction

1.1. Motivation

Autonomous driving has become a significant focus for researchers and automotive companies, raising substantial interest. One of the key challenges in this pursuit is ensuring that vehicles can accurately determine their location. This challenge becomes even more focused due to issues like signal reflections and blocked signals in urban environments, which undermine the precision of GNSS.

Various methods have been developed to address this, combining different sensors to enhance location accuracy. However, this field is still evolving; no definitive solution has emerged.

LoD2 models, representing 3D urban environments, have gained widespread availability in German cities. These models have been integrated into research and show potential for practical autonomous vehicle navigation. Meanwhile, the development of more detailed LoD3 models is also progressing. This raises an important question: can these highly detailed 3D building models significantly improve the accuracy of vehicle localization? This inquiry highlights the ongoing exploration of this field.

1.2. Challenges

Navigating in complex urban settings can pose challenges for positioning systems, primarily when vehicles depend on GNSS. As vehicles move through signal-obstructed urban canyons, the effectiveness of positioning systems can diminish. Vehicles must turn to alternative cues to determine their location in such scenarios. This leads to an interesting question: How can existing 3D maps be used to solve where a vehicle is in areas where signals are weak?

Commonly equipped with camera sensors, vehicles possess an avenue for supplementary positioning. However, capitalizing on this data is not straightforward, as the visual information encapsulated within images diverges from the structure of 3D models' non-textured surfaces. The crux of the challenge lies in harmonizing two distinct modalities: images and building models.

The main focus of this research, described in this thesis, is to find a solution to a key

question: How can detailed LoD3 models that show building facades be effectively matched with pictures from cameras to make it possible to accurately locate a vehicle? This research aims to develop creative solutions that connect these two different types of information and make them work together.

1.3. Thesis Outline

The initial segment of this thesis, as presented in chapter 2, involves a thorough exploration of the current state-of-the-art within the domain of vehicle localization. After this comprehensive review, chapter 3 becomes the focal point, detailing the specific methods employed in this study. This involves generating virtual images from LoD2 and LoD3 models, identifying and matching features, and calculating the trajectory based on these aspects.

The subsequent section is found in chapter 4, where the practical workings of vehicle localization using images are tested and evaluated. This assessment is then compared to GNSS data, as discussed in chapter 5, resulting in insightful conversations and analysis.

The final phase of this thesis is encapsulated in chapter 6, where the culmination of the findings leads to conclusions. This chapter also extends its scope toward prospects, shedding light on potential directions for subsequent research endeavors building upon the current work.

2. State of the Art

2.1. Localization Methods Based on Relative Positioning

2.1.1. Inertial Navigation

Inertial navigation is based on sensors that measure their specific changes during the movement, e.g., of a vehicle. Its unique characteristic is that it does not rely on external references. It only depends on the initial position and changes recorded by the sensor. This method has already been used for more than 20 years. With the help of a Kalman filter (or similar), the position in the future can be estimated [1]. Different sensors can be used as inertial navigation systems. Four of them are described in more detail in the following:

Accelerometers: Accelerometers measure the linear acceleration along one or more axes. Consequently, they can detect nongravitational accelerations, especially motion, orientation changes, and vibration [2]. The measurement is based on the principles of Newton's second law of motion, which states that the force applied to an object is proportional to its mass and the acceleration it experiences.

Gyroscopes: Gyroscopes "detect and measure the angular velocity of a rotational object, the deviation of a vehicle from its desired orientation" [3]. Therefore, gyroscopes are widely used in autonomous navigation systems. They are based on the principle of the conservation of angular momentum.

IMU: An IMU measures the angular velocity and the acceleration [4]. It can only measure relative positions since no world coordinates are known. Research proved that the accuracy of IMUs is not stable but drifting with time. Therefore, it is not used as a single method for localization but mostly in addition to other instruments.

Wheel odometry: Wheel encoder measure the wheel rotation angle [4]. Therefore, they are fixed on the wheels of a vehicle to estimate the distance. Electric signals representing the movement are sent out by reading out the markings of the disc. Sometimes the exact angle itself is saved. The number of those signals or the angle leads to the distance traveled. The accuracy of wheel odometry is similar to IMUs and drifting over time, which is why it is only used in combination with other methods.

2.2. Localization Method Based on Satellites

Currently, multiple global navigation satellite systems are available, like GPS of the US, Galileo of Europe, GLONASS of Russia, Beidou of China, and some regional ones, like IRNSS of India. They are all based on the same idea: Localizing a receiver on Earth by measuring the running time of a signal and calculating the receiver's distance from multiple satellites. With basic mathematics, this leads to the position of the receiver on earth [5].

The accuracy can be improved when different physical effects are addressed. For example, the ionosphere's effect must be considered and can be almost eliminated when the ionosphere-free linear combination is used [6]. For example, the final measurement accuracy along the different signals of GPS can be seen in Table 2.1. Since the L1-/L2-signal requires a lot of effort and the P-Code is only for military applications, average receivers can work with the C/A-Code and therefore have a measurement accuracy in the [m]-range [7].

GPS signal	Measurement accuracy range
C/A-Code (PRN-Code)	[m]
P-Code (PRN-Code)	[dm]
L1/L2 (carrier wave)	[cm]-[mm]

Table 2.1.: Measurement Accuracy of the Different GPS Signals. Source: [7]

Many problems regarding the accuracy apply during a GNSS measurement in urban areas. For clarity, only two essential effects are described in the following.

One effect that has to be considered is multipath. Especially in urban areas, this is a big reason why the above-stated accuracy can not be reached. Multipath means that a signal of the transmitter on board the satellite is reflected (e.g., at walls and windows). The intensity of the reflection depends on the material where the beam encounters. Consequently, the GNSS antenna receives many different signals. Therefore, the position can not be estimated with high accuracy (within the specified measurement accuracy described in Table 2.1).

Additionally, high blocks of houses around small streets cause a smaller possible field of view to the sky and, therefore, a worse configuration of satellites that can be reached (non-line of sight signal reception). This leads to worse accuracy of GNSS in urban areas.

2.3. Localization Methods Based on Images

2.3.1. Algorithms for Feature Detection

There is a handful of computer vision methods to extract features from images. In this part of the thesis, three approaches are described closer since those are the ones that are currently used in the field: SIFT, SURF, and ORB. The idea of all of them is to compare two consecutive images and find similar points despite the movement of the scene. The specifics of each method compared to the others are described in the following.

Different papers compared the performance of those three feature extractors, and other results were presented [8]. The following provides a comparison based on the data captured by 3D Mapping Solutions GmbH vehicle cameras. Therefore, the plotted data is only valid for this specific dataset and application.

SIFT



Figure 2.1.: Found Features with SIFT

SIFT was one of the first feature detectors that was developed. David G. Lowe designed an algorithm "more robust against changes in 3D viewpoint for non-planar surfaces" [9]. This is achieved because the descriptor only reacts with small changes even if relative feature positions move between the images [9]. To find feature points, SIFT computes "a histogram of locally oriented gradients around the interest point" [10].

In the used images from the dataset, 422 points were matched. The distribution of the matched features in the image can be seen in Figure 2.1. Two consecutive images can be seen in the figure, overlaying in one image. The first image is slightly blue, and the second is slightly red. If the viewer uses anaglyph 3D glasses, the image would appear 3D. The features are red-circled in the first image and green crosses in the second image. Yellow lines show the matches between two features.

SURF



Figure 2.2.: Found Features with SURF

2.3. LOCALIZATION METHODS BASED ON IMAGES

Compared to SIFT, SURF uses a different approach to detect possible feature points: a fundamental hessian matrix approximation and, consequently, the usage of integral images for image convolution [10]. Because it can be computed much faster, and the results are more accurate. In the example data, 636 points were matched using SURF, as seen in Figure 2.2.

ORB



Figure 2.3.: Found Features with ORB

The newest of the described feature detectors is ORB. It was developed in 2011 and is based on the FAST keypoint detector and the BRIEF descriptor [11]. There are 11 matched points in the current example, but the matching was limited to 1000 extracted points because otherwise, the calculating endurance is too long.

2.3.2. Algorithms for Localizing and Mapping

Structure from Motion (SfM)

Structure from Motion (SfM) is a technique to reconstruct the 3D structure of a scene and estimate the camera poses from an unordered collection of 2D images. SfM works by leveraging the relationships between features in different images and the scene's geometry to recover the scene's 3D structure and camera poses. The main steps that are performed to achieve this goal are "feature extraction and matching, followed by geometric verification [...] [as well as] triangulating scene points, filtering outliers, and refining the reconstruction using bundle adjustment (BA)" [12].

Visual Odometry (VO)

With visual odometry, a vehicle's trajectory can be estimated using a series of camera images [13]. It is advantageous over other methods due to its insensitivity to soil mechanics and lower drift rates than all but the most expensive IMUs [13]. Additionally, it works well in places where a satellite connection fails, e.g., indoors or on narrow streets. Therefore, visual odometry can be used indoors and in remote areas like other planets. It has already been used in NASA's Mars Exploration Rover Mission to "maintain an accurate onboard position estimate" [14] because IMU and wheel encoder-based odometry are insufficient in an environment like Mars. But also here on earth, VO can contribute to a full 6DOF movement estimation [13] with higher accuracy.

The trajectories estimated by visual odometry tend to drift along with increasing distance from the start point. Consequently, researchers tried to improve the concept by expanding VO ideas to another image-based localization method called SLAM [4].

Simultaneous Localization and Mapping (SLAM)

Simultaneous Localization and Mapping (SLAM) is another, more advanced technique to reconstruct reality from images. In comparison to SfM and VO, it computes the trajectory in real time and, at the same time, draws a map around the vehicle [4]. This information is then used to localize the vehicle during the rest of the journey. Therefore, SLAM achieves higher accuracies, especially for round trips. The actual values substantially deviate since the accuracy accumulates over time [15]. Consequently, a round trip's start and end points are far away, and the system is not perceiving the connection. Since SLAM is simultaneously mapping the environment and updating the map during driving, the current point is automatically corrected by the data from the positions that were already calculated before. The system automatically optimizes the trajectory on-the-fly.

2.4. Localization Methods Based on LoD2 Models

A 3D city model can be used to georeference the vehicle properly. For this, geometrical information from the buildings surrounding the vehicle is extracted and matched with points in the images to scale, localize and correctly map the trajectory. In LoD2, this geometrical information includes the edges of the buildings. In LoD3, facade details and edges of windows can be helpful references. There are a few papers which already tested the usage of LoD-1 and LoD2 models for vehicle localization:

Vogel et al. work on localizing objects in "complex indoor as well as inner-city outdoor environments" [16]. For this, they modify an iterated extended Kalman filter (IEKF) to be able to integrate additional information into it. This information is observed by an IMU, a laser scanner, and primary structural conditions (e.g., walls). Due to the "use[age] of geometric circumstances in the direct environment of the MSS [...] [they can] provide a more precise and reliable georeferencing" [16]. Their idea is refined in later papers.

In 2021, Moftizadeh et al. study the possible applications of 3D city models for UAVs [17]. They aim to improve the iterative extended Kalman filter, developed by [16] to their needs. Points generated by a laser scanner are assigned to a plane of the 3D city model or a cell of the digital terrain model to optimize the localization by calculating the 2D Euclidean distance [17]. This technique creates points in the same coordinate system and therefore helps to estimate the UAV's position in the real world.

Lucks et al. introduce a similar approach for improving a vehicle's trajectory on the ground [18]. They match the point cloud with an LoD-1 using a point-to-plane iterative closest point method. With the result, they can optimize the trajectory which GNSS measured. Their idea is to only use 3D-City models publicly available via geo-web services [18].

3. Methodology

3.1. Overview of the Final Workflow

The workflow of the developed method can be seen in Figure 3.1. This workflow is used on the LoD2 and the LoD3 model to compare both results.

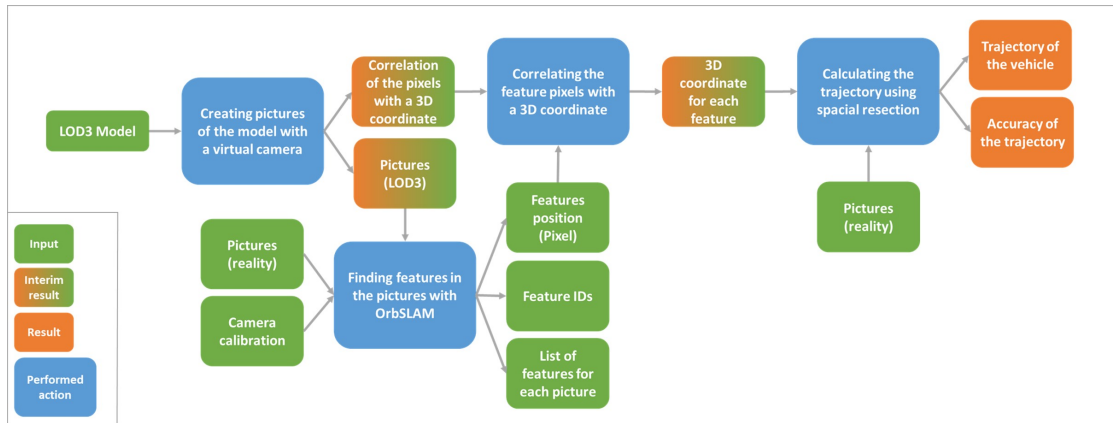


Figure 3.1.: Workflow

The project is divided into four main parts. First, virtual pictures of the LoD models are created. The resulting images are then used to find features in the corresponding image taken from reality. For this, the ORB detector is used. The generated 2D-image coordinates are correlated with a 3D coordinate by benefiting from the LoD model. In the end, these coordinates are needed to estimate the camera position for every single image with spatial resection. A trajectory can be calculated and compared with the GNSS data. The code to run the developed method can be found in the GitHub repository "LoD3ForLocalization"; see [19].

3.2. Creating Virtual Images of the LoD3 Model

For the first step, the virtual images are created using ray casting. To work with the ray casting algorithm, a mesh is generated from the .obj file of the LoD models since all results are based on the hit of a triangle by virtual rays. The algorithm creates those virtual rays and sends them through a virtual camera, preferably in the direction of the model. Every time a ray hits a point, the corresponding triangle and the barycentric coordinates of the exact hit point (in the triangle) are saved. Therefore, the 3D coordinates in the real world can be calculated by only knowing the 2D coordinates of the virtual image. The calculation is described in section 3.4.

Moreover, the virtual camera's positioning point and viewing direction are needed (see Figure 3.2). As an approximation solution, the position is taken from the GNSS data of the current corresponding real-world image. On top, the camera's height above the GNSS antenna must be considered, leading to GNSS values adapted to the camera position. The camera is pointing to the adapted GNSS position of the consecutive image. Afterward, the orientation of the camera needs to be adjusted. For this, the calibration file is used: The angles for roll, pitch, and yaw are required to approximate the point close to the GNSS position in consideration of the tilt of the camera. A visual example of pitch can be seen in Figure 3.2. The approximation is calculated as follows:

$$dy[m] = r_{GNSS} \cdot dy[^\circ] \cdot \frac{\pi}{180^\circ} \quad (3.1)$$

All in all, an overview of the above-described virtual setup can be seen in Figure 3.2:

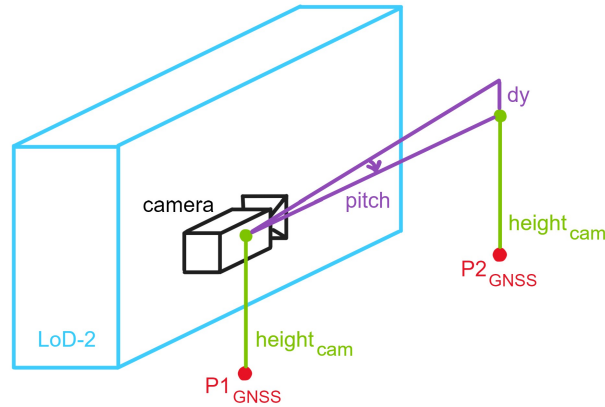


Figure 3.2.: Virtual Setup for Ray Casting

3.2. CREATING VIRTUAL IMAGES OF THE LOD3 MODEL

After applying the Ray Casting algorithm, the results are available in a tensor. There are four results: the distance ('t_hit'), the geometry IDs, the primitive IDs, the primitive normals, and the barycentric coordinates ('primitive_uv's'), for an example, see Figure 3.3.

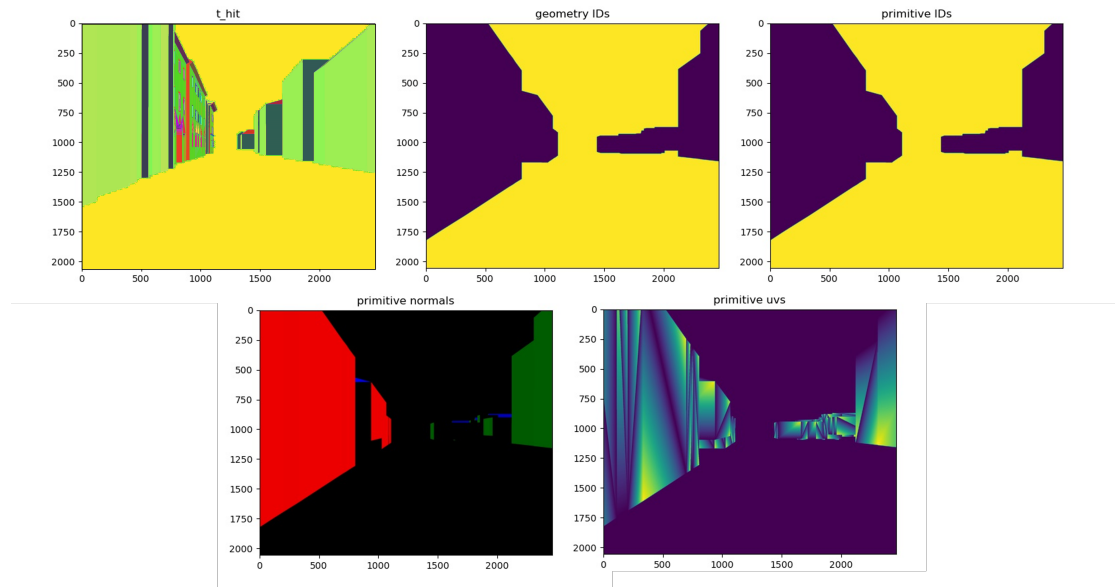


Figure 3.3.: Ray Casting Results for LoD2

The virtual images are generated on the images, which include an adjustment of the primitive normals ('primitive_normals') because then the differences between two buildings are visible. Otherwise, both buildings would have the same color and blur into each other since the building in front would hide the building behind it. Therefore, some information regarding this important edge would get lost for feature matching. The adjustment (absolute value, no negative values of the normals allowed) is applied since the exact value is unimportant for the virtual images. This is necessary so that every side of the building has a unique color. This will optimize the found features and, therefore, the results.

An example for the LoD3 models is visualized in Figure 3.4. The LoD3 ray casting images are more detailed, due to the additional information on the model, especially regarding windows and roof eaves. The underpass of the model causes the colorful triangles in the example. The methods in chapter 4 test whether the color coding is confusing for the method.

3.3. FEATURE MATCHING

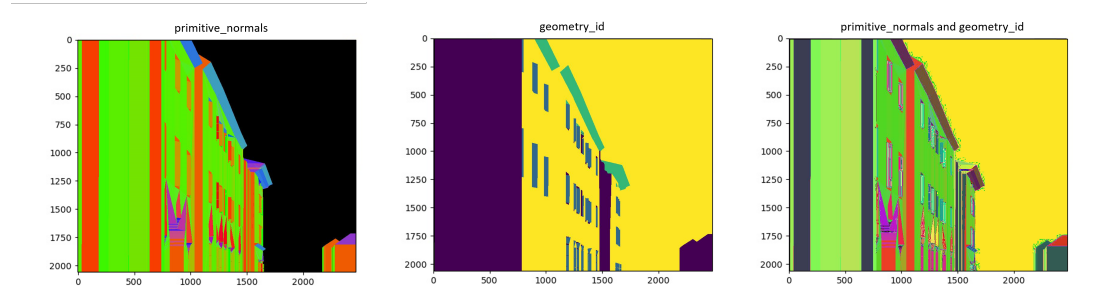


Figure 3.4.: Ray Casting Results for LoD3

3.3. Feature Matching

The feature matching is performed on images with fewer details. Therefore, the images become more abstract and only focus on important information. For this, the images are matched against themselves (the virtual and the image from reality).

The next step is done for the image of the real world, as well as for the one of the virtual camera. First, another abstract, virtual feature image is created and implemented as a matrix with the same values for every pixel. If features were found in matching the images against themselves, this pixel is colored differently. This is realized by assigning a different value to this pixel in the matrix. The image, therefore, only contains information about the essential points of the image before.

Afterward, these newly created feature images are matched with an ORB-feature detector again. An overview of the idea is visualized in Figure 3.5.

3.3. FEATURE MATCHING

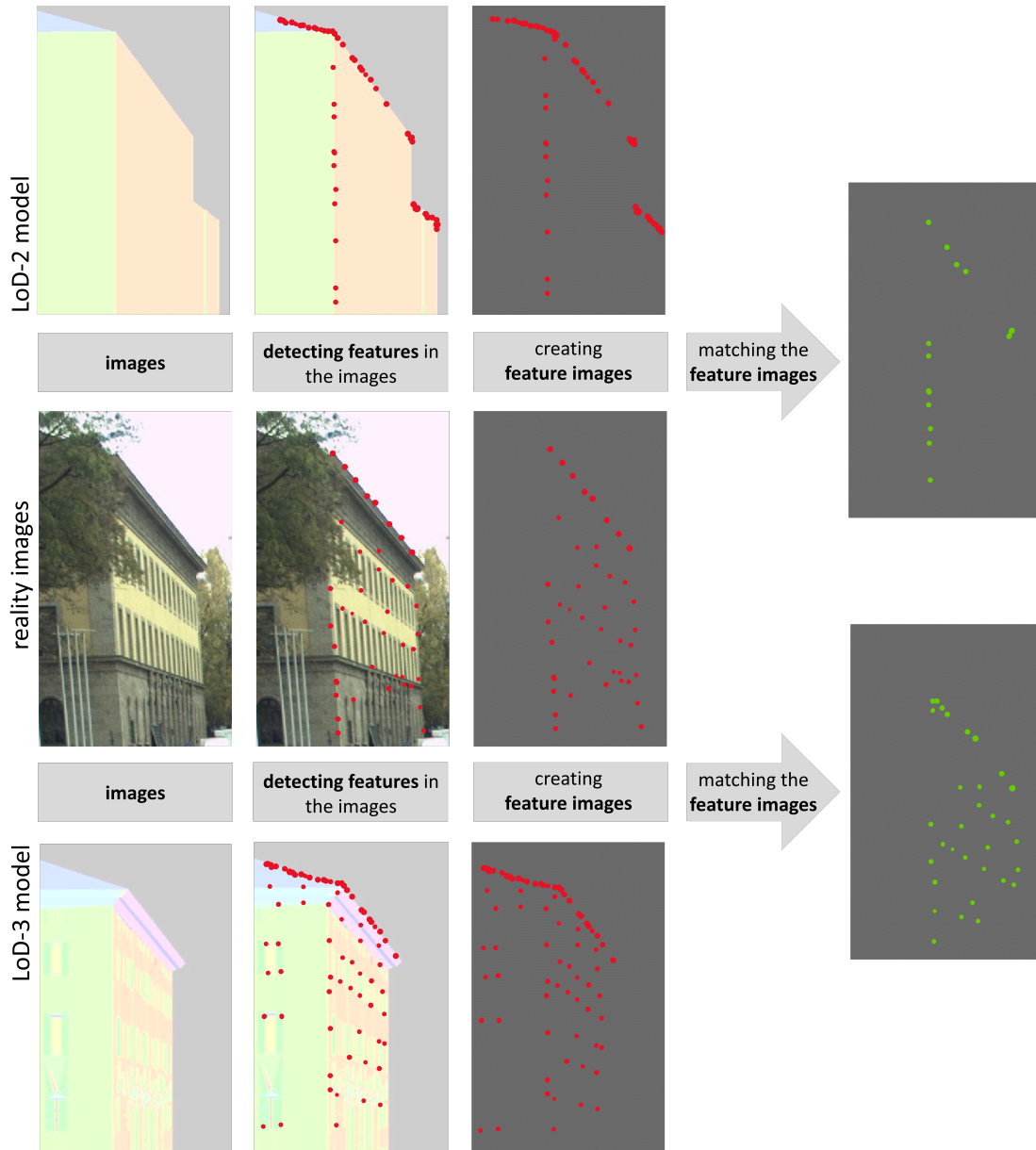


Figure 3.5.: Workflow of the Generation of the Feature Images

3.4. Correlating the Features with a 3D-Coordinate

This part of the thesis describes how the 3D coordinates of a feature point are extracted from the LoD models. In the beginning, the triangle IDs the rays hit are saved. Then, the corresponding triangles in the mesh are found. With this, it is possible to see which vertices belong to a triangle that was hit. From the IDs of those vertices, the 3D coordinates from the vertex positions can be read out in the mesh. Finally, the exact point needs to be weighted by the vertices of its triangle because only the relative positions from the vertices are known. The results only return two barycentric coordinates for each hit point. This is because the sum of the three coordinates is 1:

$$1 = u + v + s \quad (3.2)$$

This means that s can be directly derived from u and v . The weighting to receive the final coordinates is calculated as follows:

$$P = u * P_{vertex1} + v * P_{vertex2} + s * P_{vertex3} \quad (3.3)$$

3.5. Calculating the Trajectory

The vehicle's trajectory is simultaneously calculated by driving and reading the generated images. This is possible with the usage of spatial resection. Spatial resection is a set of statistical formulas to compute the accuracy of observations by finding a model that fits them best. Consequently, the accuracy of the observations and related values can be calculated afterward. In this case, the camera position is estimated while the observations are optimized at the same time. The position calculation is performed with the help of the photogrammetrical co-linearity equations, which can be seen in Equation 3.4 and Equation 3.5.

$$x = \hat{x}_0 + z \frac{(r_{11}(X - \hat{X}_0) + r_{21}(Y - \hat{Y}_0) + r_{31}(Z - \hat{Z}_0))}{(r_{13}(X - \hat{X}_0) + r_{23}(Y - \hat{Y}_0) + r_{33}(Z - \hat{Z}_0))} \quad (3.4)$$

$$y = \hat{y}_0 + z \frac{(r_{12}(X - \hat{X}_0) + r_{22}(Y - \hat{Y}_0) + r_{32}(Z - \hat{Z}_0))}{(r_{13}(X - \hat{X}_0) + r_{23}(Y - \hat{Y}_0) + r_{33}(Z - \hat{Z}_0))} \quad (3.5)$$

For the calculation, are six values to be determined, representing the camera's position and orientation: $X_0, Y_0, Z_0, \omega, \phi, \kappa$. Consequently, for the solution, at least six corresponding points are needed. To get even better accuracy, more corresponding points are preferred. The spatial resection is performed as follows. First, the image coordinates of the features are transformed from [pixel] to [m].

A direct linear transformation generates the approximate camera orientation values. Input parameters are at least six corresponding points. The approximate camera position is taken from the corresponding GNSS point. The approximate values are needed because the spatial resection needs starting points to optimize. Otherwise, the algorithm might run into a local minimum and keeps iterating in an infinite loop.

In the optimization loop, the derivations of the A-matrix are computed. This is necessary because the refinements of the observations for the best-fitting model are calculated with the help of this matrix. The A-matrix has the size of $[n \times m]$, while n is the number of observations and m is the number of values to be determined.

The values that are to be determined are estimated in every iteration by calculating the following:

$$\delta\hat{x} = \frac{(A^T * P_{bb} * A)}{(A^T * P_{bb} * w)} \quad (3.6)$$

Where A is the already described A-matrix. P_{bb} is a matrix that contains weights. Those weights decide how important an observation is, e.g., if the measurement is probably more precise than others because of the geometrical position. The w -vector contains the current errors between the approximated $\delta\hat{x}$ and the actual observations. The optimized observation values are computed by:

$$\delta\hat{v} = A * \delta\hat{x} - w \quad (3.7)$$

4. Experiments

4.1. Dataset

The experiments are conducted on the datasets depicting the TUM campus in Munich, Germany. The image data was received from 3D Mapping Solutions GmbH. The camera has the following characteristics:

camera detail	value
camera on the vehicle	9
field of view	54.686033 °
width	2464
height	2056

Table 4.1.: Camera Details

For Ray Casting these camera details are needed. The field of view along the width is calculated by using the camera constant c :

$$for[m] = \arctan\left(\frac{width}{c} \cdot 2 \cdot 180^\circ\right) \quad (4.1)$$

Since the LoD2 models are freely available for Munich, they are downloaded through the Geodata portal of Bavaria [20]. The LoD3 models are developed by the Chair of Photogrammetry and Remote Sensing and the Chair of Geoinformatics at the Technical University of Munich [21]. Different areas where all models and images are available are tested in this thesis (Theresienstraße 90-100, Arcisstraße 21, Gabelsbergerstraße 39-55). Consequently, it was focused on the streets around the campus in the city center of the Technical University of Munich.

In Figure 4.1, the used buildings and the three testing routes can be seen. The numbers are coding for the last two digits of the GML IDs by the Landesamt für Digitalisierung, Breitband und Vermessung (LDBV). The buildings with numbers are the ones that are available as LoD3 and LoD2 models. All other buildings visible in the image are additionally available as LoD2 models.

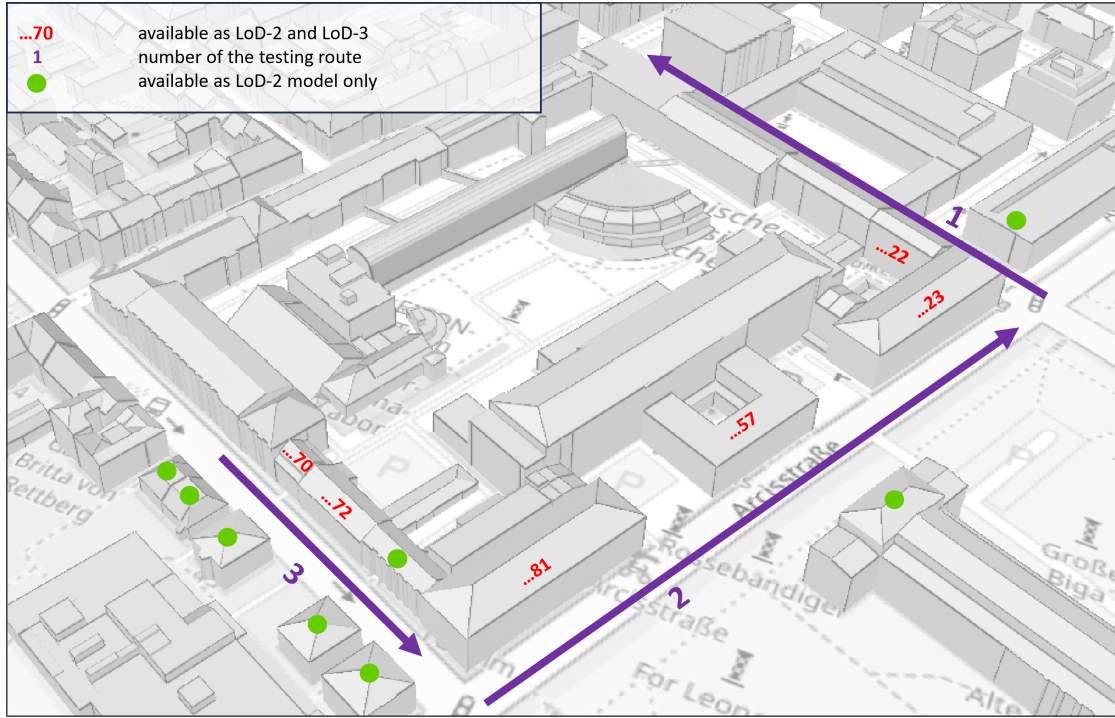


Figure 4.1.: Testing Area. Adopted from: [22]

As LoD3 models are not available for the entirety of the testing area, a hybrid approach involving a combination of LoD2 and LoD3 models is adopted in this scenario. This hybrid approach ensures a balanced distribution of potential points and promotes an effective configuration; for a more detailed description, see section 5.1. Notably, there are no instances in the testing area where LoD3 models are present on both sides of the street nearby. The missing LoD3 models are supplemented from the LoD2 dataset as a solution. Notably, the same models from the LoD2 dataset are used for experiments involving solely LoD2 models. This allows a direct evaluation of the influence of the LoD3 compared to the usage of only LoD2 models.

4.2. Different Approaches for Feature Matching

The feature matching was performed on five different pillars. Each approach is described in more detail in the following.

4.2.1. Corresponding Image-Pairs of Different Types

The idea of this approach is to find features from image pairs that are not the same type. This means that one virtual image is matched with one image of reality. Both images are taken from the same GNSS point. The results show only a median of 9-18 suitable feature matches for each image pair. Furthermore, most do not belong to the same point on the facade point on the model, as seen in Figure 4.2.

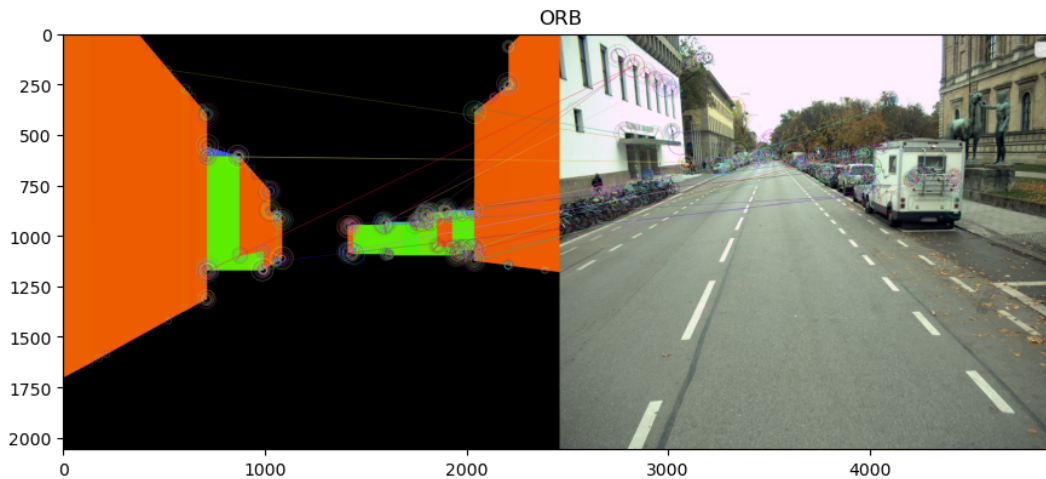


Figure 4.2.: Found Features in a) Virtual Generated Image b) Real Image

In Figure 4.2, the matches found in the images are drawn in circles. A line is connecting the features which are matched with each other. It is visible that the matched points do refer to different points since the lines connecting the features in both images do not have approximately the same orientation. In an ideal situation, they would be almost parallel and have the same length. In this case, their angles are different, indicating they do not connect the same points.

4.2.2. Segmented Images with Machine Learning

Matching real images with virtual images presents a challenge due to the presence of disruptive elements that are not shared between the two image types. To mitigate this issue, the approach involves segmenting the real images. To achieve this, an algorithm sourced from 3D Mapping Solutions GmbH is employed. It is built on the segformer-network, which is available through the mmsegmentation framework [23]. This algorithm generates an output image where distinct elements such as buildings, cars, and pedestrians are each assigned a unique color, see Figure 4.3.

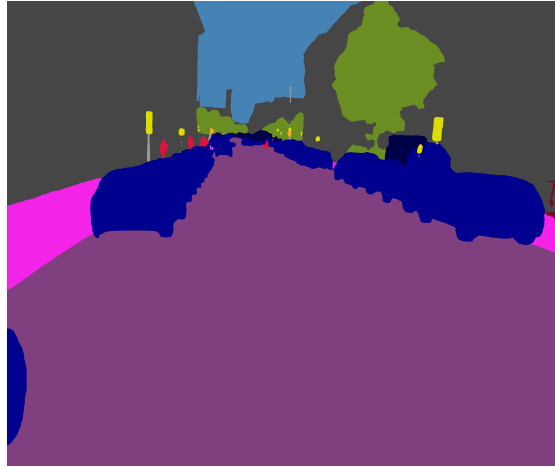


Figure 4.3.: Output of the Segmentation

However, direct matching of these segmented images with the unprocessed real images is not feasible. The uniform coloration of buildings in the segmented images blurs the corner edges between two buildings, rendering them indistinct and thus less visible. To address this, a method is devised wherein the segmented images act as masks for the real images. This process involves isolating the building areas from the real images using the segmented images as guides. Consequently, only the building-related parts of the real image are retained and matched with their virtual counterparts.

This strategic approach effectively eliminates any potential disruptions from extraneous objects that could potentially result in erroneous matches.

4.2.3. Sobel-Filter and Canny Edge Detection

The optimal approach to feature matching focuses solely on features along building edges, including structures like building facades and window edges. A combination of techniques is employed to achieve this, including using Sobel filters and Canny edge detection.

In instances where it is desirable to exclusively match buildings, applying a bounding box to actual images proves effective. These filters are harmonized with the segmented images detailed in subsection 4.2.2 to ensure precision. This strategic combination prevents the extraction of excessive edges from real images, ensuring that only relevant objects for vehicle localization are considered. Additionally, the results for Sobel-X and Sobel-Y are combined to one image including both. The resultant Sobel-filtered and Canny-edge-detected images exhibit the following characteristics:

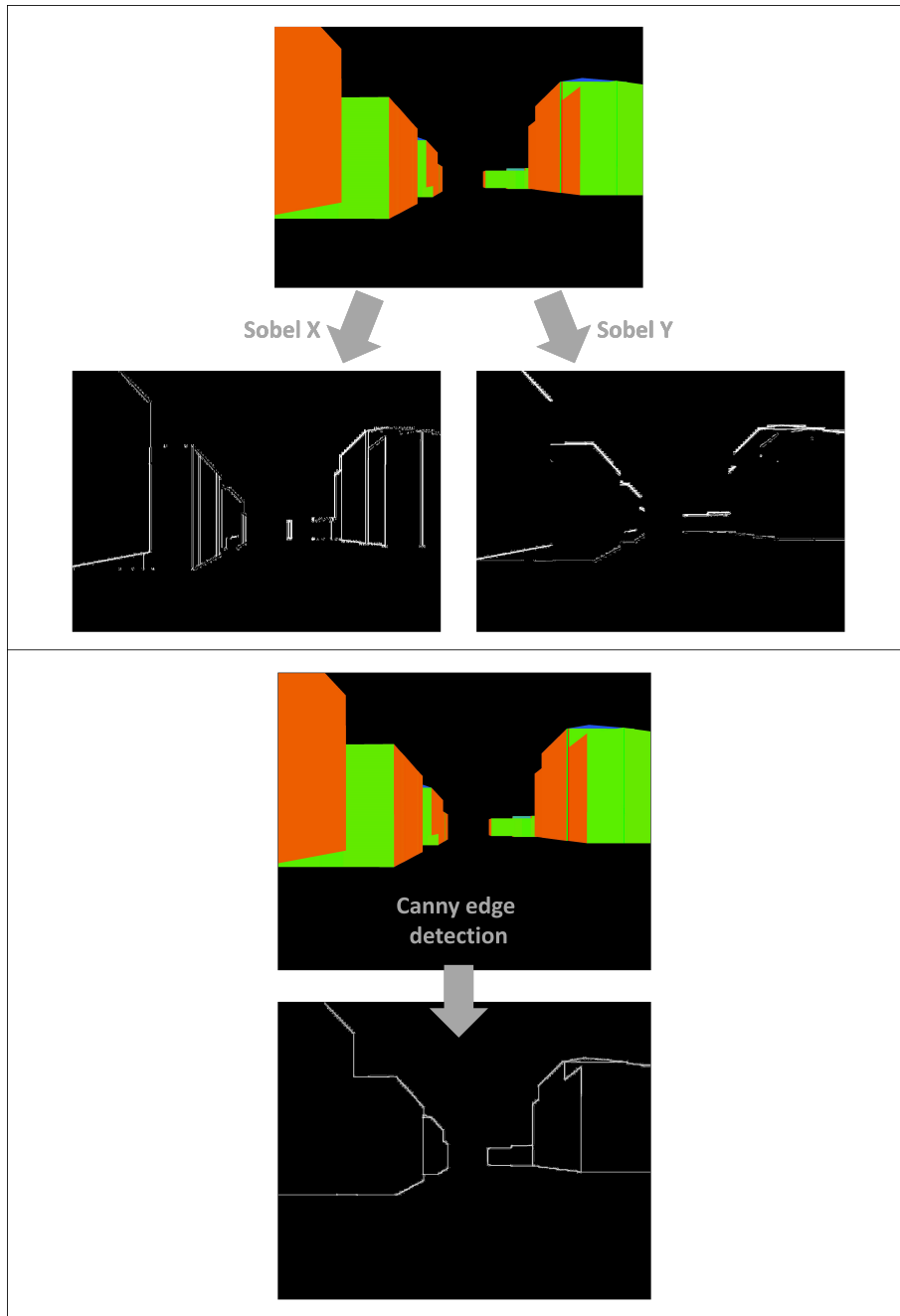


Figure 4.4.: a) Sobel-Filter and b) Canny Edge Detection on the Images

4.3. Results

4.3.1. Number of Features

The different approaches lead to different results regarding the number of found features. These features represent those that can be successfully matched between two images while simultaneously being positioned on the appropriate LoD model rather than the background. A comprehensive comparison for each model, namely LoD2 and LoD3, is presented across different testing areas in Table 4.2, Table 4.3, and Table 4.4. Within each testing area, the selection pertains to the median of all tested images. The best result, comparing LoD2 and LoD3 for each experiment is written in bold. The complete evaluation of every single image is enclosed in Appendix A in the Appendix.

	LoD2	LoD3
Corresponding images	17	18
Feature images	20	50
Sobel-filter	14	13
Canny edge detection	21	21
Mask	18	18
Mask and Sobel-filter	21	11
Mask and Canny edge detection	34	22

Table 4.2.: Number of Found Features (Median) in the Testing Area 1

	LoD2	LoD3
Corresponding images	12	9
Feature images	20	65
Sobel-filter	10	10
Canny edge detection	8	14
Mask	15	12
Mask and Sobel-filter	13	14
Mask and Canny edge detection	21	27

Table 4.3.: Number of Found Features (Median) in the Testing Area 2

4.3. RESULTS

	LoD2	LoD3
Corresponding images	15	18
Feature images	20	47
Sobel-filter	13	15
Canny edge detection	14	20
Mask	13	20
Mask and Sobel-filter	15	17
Mask and Canny edge detection	26	21

Table 4.4.: Number of Found Features (Median) in the Testing Area 3

4.3.2. Deviation from the Trajectory

Additionally, the deviation between the trajectory and the corresponding GNSS point is compared. By this, the exactness of the calculated camera point and, therefore, the correctness of the feature matching is evaluated. Again, the accuracy differences for LoD2 and LoD3 are in focus; the best value is highlighted bold.

	LoD2	LoD3
Corresponding images	105.69m	85.19m
Feature images	210.56m	188.18m
Sobel-filter	158.74m	75.55m
Canny edge detection	120.17m	103.65m
Mask	105.47m	110.42m
Mask and Sobel-filter	106.95m	46.29m
Mask and Canny edge detection	129.40m	98.08m

Table 4.5.: Deviation from the Corresponding GNSS Point (Median) in Testing Area 1

4.3. RESULTS

	LoD2	LoD3
Corresponding images	151.79m	141.95m
Feature images	321.76m	229.25m
Sobel-filter	139.46m	118.80m
Canny edge detection	133.99m	66.50m
Mask	135.54m	87.13m
Mask and Sobel-filter	126.72m	101.28m
Mask and Canny edge detection	171.89m	88.00m

Table 4.6.: Deviation from the Corresponding GNSS Point (Median) in Testing Area 2

	LoD2	LoD3
Corresponding images	142.32m	178.76m
Feature images	329.25m	169.13m
Sobel-filter	72.00m	171.05m
Canny edge detection	67.62m	193.97m
Mask	60.44m	215.65m
Mask and Sobel-filter	93.67m	239.06m
Mask and Canny edge detection	214.45m	183.57m

Table 4.7.: Deviation from the Corresponding GNSS Point (Median) in Testing Area 3

4.3.3. Accuracies of the Calculated Camera Position

The accuracy of the calculated camera position is presented in the following tables. The accuracies per cell are structured as $[\sigma_X \mid \sigma_Y \mid \sigma_Z]$.

	LoD2	LoD3
Corresponding images	35.81m	15.26m
	36.39m	46.10m
	44.25m	21.11m
Feature images	81.72m	111.87m
	50.40m	152.39m
	74.92m	94.45m
Sobel-filter	66.13m	51.23m
	67.34m	58.56m
	65.85m	31.64m
Canny edge detection	48.71m	35.82m
	50.27m	47.18m
	52.06m	27.31m
Mask	19.93m	56.26m
	32.32m	44.57m
	29.15m	48.74m
Mask and sobel-filter	55.96m	65.78m
	74.12m	23.43m
	59.12m	42.22m
Mask and canny edge detection	59.45m	38.27m
	92.93m	55.16m
	50.31m	42.67m

Table 4.8.: Standard Deviation of the Camera Position (Median) in Testing Area 1

4.3. RESULTS

	LoD2	LoD3
Corresponding images	48.02m	17.49m
	44.22m	41.67m
	58.98m	49.33m
Feature images	130.94m	168.78m
	191.27m	169.88m
	194.87m	158.22m
Sobel-filter	93.47m	21.96m
	76.02m	26.54m
	51.87m	15.89m
Canny edge detection	43.62m	48.33m
	24.39m	52.87m
	38.84m	33.06m
Mask	9.62m	13.77m
	13.59m	25.69m
	14.63m	10.12m
Mask and sobel-filter	67.45m	94.36m
	91.99m	85.56m
	96.01m	80.71m
Mask and canny edge detection	37.74m	42.08m
	40.91m	58.02m
	40.69m	27.19m

Table 4.9.: Standard Deviation of the Camera Position (Median) in Testing Area 2

4.3. RESULTS

	LoD2	LoD3
Corresponding images	71.37m	40.05m
	76.23m	66.23m
	80.26m	77.21m
Feature images	171.01m	21.14m
	127.70m	38.17m
	104.11m	21.44m
Sobel-filter	59.78m	40.71m
	43.54m	65.81m
	42.67m	35.07m
Canny edge detection	24.98m	9.35m
	33.31m	11.62m
	19.12m	6.07m
Mask	38.90m	20.10m
	33.51m	60.34m
	40.14m	27.97m
Mask and sobel-filter	21.05m	33.62m
	23.25m	47.88m
	19.21m	44.98m
Mask and canny edge detection	159.73m	7.83m
	168.19m	13.24m
	180.55m	5.19m

Table 4.10.: Standard Deviation of the Camera Position (Median) in Testing Area 3

5. Discussion

5.1. Evaluation of the Developed Methodology

The developed method performs well. The method needs images, semantic building models, and GNSS information for the initial location as inputs and returns a trajectory, including its accuracy. The steps of the performed actions that have to be performed are implemented successfully.

First, virtual images were created via ray casting. Then, features were found in and matched between the virtual and real images. Since the 3D coordinate of every pixel in the virtual images can be computed from the ray casting results, every feature match correlates with a real-world coordinate. Ultimately, these correlations are used to calculate the trajectory using spatial resection. The most reliable method for feature matching, using the feature images, was chosen from those tested in chapter 4.

No complete SLAM approach is implemented since this is beyond the scope of this thesis. This means that two consecutive images are only compared against each other, like in VO. The developed map of the environment is not updated during the drive.

Finding an algorithm in digital image processing that matches features with a reliability of around 100% was challenging. As described in chapter 4, different approaches, including basic and innovative image processing tools, were tested to get the best results in feature matching. The results are similar: Many features are found between the two images, but the matching was complex. The situation is especially challenging for LoD3, which was unexpected: More features can be found in LoD3 than LoD2, but this also increases the false matching.

As seen in Figure 5.1, many features were found in the image pairs, which are visible as circles. The matches between two features are shown by connecting lines. In an ideal situation, those lines will nearly have a similar angle and length since the scene's configuration is approximately the same in both images. However, this does not apply to the example: In this case, the connections point in the same direction, but features from the left side of one image are matched with the right side of the other image. This is the reason for bad accuracies, described in more detail in section 5.2.

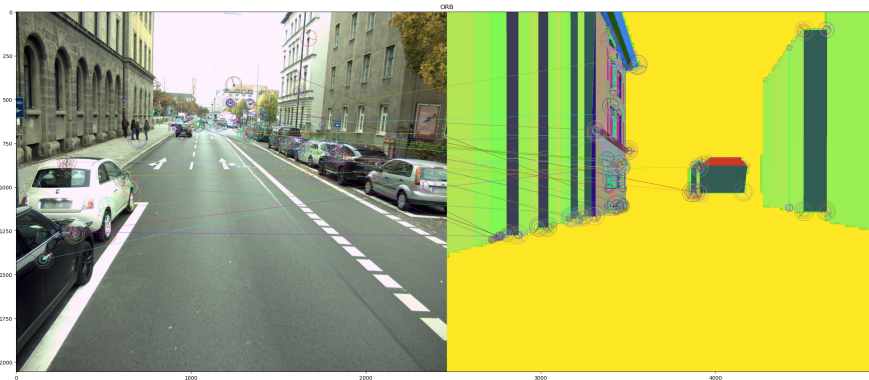


Figure 5.1.: Found Features in a) Real Images b) LoD3

5.2. Evaluation of the Achieved Accuracies

Three testing areas were chosen to compare different situations that can occur during driving. The first testing area includes an underpass. The remarkable thing about this is that underpasses are not visualized in a LoD2 model. Instead, the vertical wall is drawn down to the floor; see Figure 5.2. This is a huge problem when those models are used for localizing autonomous cars.

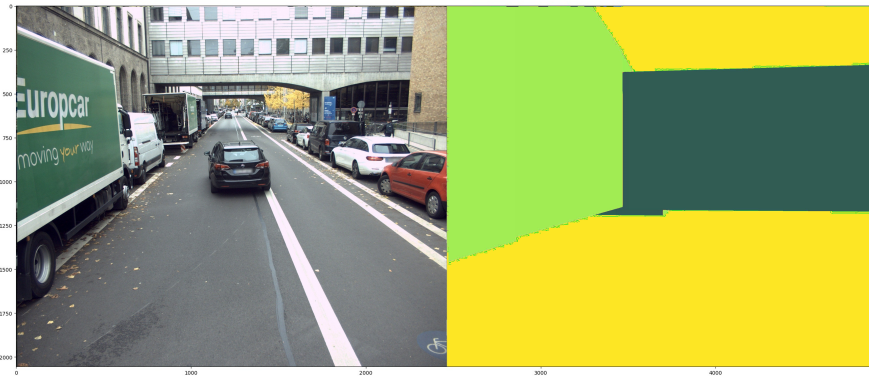


Figure 5.2.: Underpasses in a) Reality b) LoD2

The second testing area includes a different challenge in localization based on 3D city models and images: Buildings are only visible on one side of the street. The other side is occupied by trees or other vegetation. This leads to a bad configuration for estimating the trajectory because possible features can only be found on one side of the trajectory, as seen in Figure 5.3.

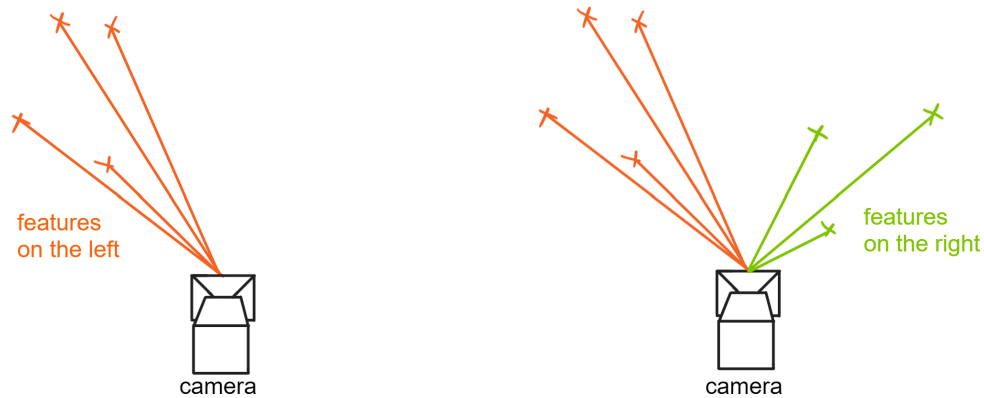


Figure 5.3.: Visualization of the Configurations

The angles of the features to the camera in the configuration of the left are similar, which causes a more unreliable positioning. In the configuration on the right, the features are distributed over the viewing area. By this, the positioning error can be reduced. Nevertheless, the right configuration can not be assured during the journey of an autonomous vehicle. Therefore, the different testing areas will show how well the idea of using images and 3D city models for localization performs in other situations.

Testing area 3 seems to be the best case for building-based trajectory calculations, since buildings with clear facade patterns cover both sides of the streets.

Analyzing the tables in chapter 4, the tests are showing that the method is, on average, resulting the same or more features for LoD3, a smaller deviation from the corresponding GNSS point and a smaller standard deviation.

In testing area 1, LoD3 works better for positioning because the underpasses lead to great problems for LoD2. Close to the underpass, the localization with images is failing since no features can be found anymore.

More features lead to a more reliable estimation of the trajectory point, which can especially be seen in testing area 2. Only one side is covered by buildings, but the LoD3 model still results in a smaller deviation from the GNSS point. The reason for this is that it is important in this area to have more features on the walls, since only one side of the street can be used for positioning. LoD3 reaches a higher number of features, which is why the standard deviation of the camera point is better. The deviation from the corresponding GNSS point is worse compared to the other testing areas due to the bad configuration, as described above.

In testing area 3, the deviation from GNSS is smaller for LoD2 than for LoD3. This is

because more features also cause more incorrect allocations, as described above. At the same time, more found features provide a better distribution in the image and therefore create a better standard deviation. Considering the standard deviation of the camera position for the evaluation, LoD3 is favorable in testing area 3.

In general, the deviation of the calculated camera position looks slightly better in LoD3 compared to LoD2. A reason for the deviation from the GNSS point is an imprecise calculation of the 3D coordinates. The exact coordinates are weighted by the barycentric coordinates in the triangle. Consequently, each triangle vertex belongs to exactly one of the barycentric coordinates u, v, s . This depends on the sequence in which the triangle coordinates are saved in the mesh. The order of the vertices is a requirement that is currently under great research for LoD2 and LoD3 models. The topology for such models has to be consistent in every model, e.g., in the right-hand view.

A colored visualization of the underpasses can also be caused by this problem since the normals of the triangles can show to the other direction, compared to the triangle next to it, depending on the triangle's topology. The method developed in this thesis works under the assumption that the models are correct and the vertices are saved in the right-hand view.

The calculation of the 3D coordinates and the problem of precise feature matching need to be improved to achieve accuracies that can be applied in real autonomous vehicles.

5.3. Comparison with GNSS Data

The program works best in situations, where buildings cover both sides of the street. The higher the buildings, the more details can be found for feature matching. Additionally, narrow streets are advantageous, because the buildings are closer to the camera and can be captured in more detail.

In contrast, GNSS data is most accurate in urban environments when surrounded by only low buildings. Narrow streets lead to position errors. Consequently, the localization with images and LoD3 models is advantageous over the usage of GNSS in urban areas.

The developed algorithm fails in urban areas when buildings are only available on only one side of the street. In this case, GNSS is working more precisely.

6. Conclusions and Outlook

6.1. Key Findings

Overall, positioning with GNSS and based on images and 3D city models are like counterparts: where one method fails, the other method has advantages. For example, locating in narrow streets with high buildings is beneficial using the method developed in this thesis.

The combination of both methods thus shall reach in the best results.

6.2. Real-World Applications and Implications

Reliable navigation in urban areas is a prerequisite for the economy, safety, efficiency, and quality of life. Another milestone for using autonomous vehicles is achieved if this condition is met.

Image-based localization combined with 3D city models can also bring many advantages in other areas: drones, which may deliver our packages in the future, also require secure positioning between canyons of houses. It is essential to secure safety in navigation to fulfill the requirements of drone regulations.

Helicopters must be able to land in cities in the case of emergencies. The developed method can help them land safely between hospital buildings without positioning errors due to the lost GNSS signal.

Additionally, for many applications using robots, localization without GNSS is needed. Robots often work inside buildings where no GNSS signal is reachable. Navigating with images is really helpful to estimate a right and reliable position.

6.3. Future Research Directions

The basic idea of image-based localization in combination with enhanced 3D city models is interesting for the future of navigation in urban environments and must be continued. The biggest challenge is the sufficient matching of features between the two distinct modalities: images and building models. Further research should optimize the matching process to ensure the corresponding features are matched as well as the topology of these models. A universal way to structure the saved vertices has to establish e.g., the right-hand view.

Additionally, the best solution will be to combine images from different methods to achieve the most promising result. Future research can work on the approach to train a neuronal network for recognizing windows and doors. The resulting images can then be combined with the output of a Sobel filter so that the edges of the buildings will be visible.

LoD3 models produce more features. Once the challenge to match those features correctly is faced, the positioning accuracy will most likely be enhanced compared to LoD2.

List of Figures

2.1. Found Features with SIFT	5
2.2. Found Features with SURF	6
2.3. Found Features with ORB	7
3.1. Workflow	10
3.2. Virtual Setup for Ray Casting	11
3.3. Ray Casting Results for LoD2	12
3.4. Ray Casting Results for LoD3	13
3.5. Workflow of the Generation of the Feature Images	14
4.1. Testing Area. Adopted from: [22]	18
4.2. Found Features in a) Virtual Generated Image b) Real Image	19
4.3. Output of the Segmentation	20
4.4. a) Sobel-Filter and b) Canny Edge Detection on the Images	21
5.1. Found Features in a) Real Images b) LoD3	29
5.2. Underpasses in a) Reality b) LoD2	29
5.3. Visualization of the Configurations	30

List of Tables

2.1. Measurement Accuracy of the Different GPS Signals. Source: [7]	4
4.1. Camera Details	17
4.2. Number of Found Features (Median) in the Testing Area 1	22
4.3. Number of Found Features (Median) in the Testing Area 2	22
4.4. Number of Found Features (Median) in the Testing Area 3	23
4.5. Deviation from the Corresponding GNSS Point (Median) in Testing Area 1	23
4.6. Deviation from the Corresponding GNSS Point (Median) in Testing Area 2	24
4.7. Deviation from the Corresponding GNSS Point (Median) in Testing Area 3	24
4.8. Standard Deviation of the Camera Position (Median) in Testing Area 1 .	25
4.9. Standard Deviation of the Camera Position (Median) in Testing Area 2 .	26
4.10. Standard Deviation of the Camera Position (Median) in Testing Area 3 .	27

Bibliography

- [1] S. Sukkariéh. “Low Cost, High Integrity, Aided Inertial Navigation Systems for Autonomous Land Vehicles.” PhD thesis. The University of Sydney, 2000.
- [2] A. Hines, A. Nelson, Y. Zhang, G. Valdes, J. Sanjuan, J. Stoddart, and F. Guzmán. “Optomechanical Accelerometers for Geodesy.” In: *Remote Sensing* 14.17 (Sept. 2022), p. 4389. ISSN: 2072-4292. DOI: 10.3390/rs14174389. URL: <http://dx.doi.org/10.3390/rs14174389>.
- [3] X. Zhuang and L. Zhou. *Gyroscopes*. Rijeka: IntechOpen, May 2020.
- [4] X. Gao and T. Zhang. *Introduction to Visual SLAM: From Theory to Practice*. Singapore: Springer Nature Singapore Pte Ltd., 2019.
- [5] U. Hugentobler. *Lecture notes in “2. Beobachtungsgleichungen” (Module: Satellitegeodesy, TUM)*. Nov. 2022, Semester 5.
- [6] U. Hugentobler. *Lecture notes in “5. Differenzbildung und Linearkombinationen” (Module: Satellitegeodesy, TUM)*. Jan. 2023, Semester 5.
- [7] U. Hugentobler. *Lecture notes in “4. GNSS-Signale” (Module: Satellitegeodesy, TUM)*. Nov. 2022, Semester 5.
- [8] M. Bansal, M. Kumar, and M. Kumar. “2D object recognition: a comparative analysis of SIFT, SURF and ORB feature descriptors.” In: *Multimedia Tools and Applications* 80 (2021), pp. 18839–18857.
- [9] D. G. Lowe. “Distinctive Image Features from Scale-Invariant Keypoints.” In: *International Journal of Computer Vision* 60(2) (2004), pp. 91–110.
- [10] H. Bay, A. Ess, T. Tuytelaars, and L. Van Gool. “Speeded-Up Robust Features (SURF).” In: *Computer Vision and Image Understanding* 110 (2008), pp. 346–359.
- [11] E. Rublee, V. Rabaud, K. Konolige, and G. Bradski. “ORB: An efficient alternative to SIFT or SURF.” In: *2011 International Conference on Computer Vision*. 2011, pp. 2564–2571.
- [12] J. Schönberger and J.-M. Frahm. “Structure-from-Motion Revisited.” In: June 2016. DOI: 10.1109/CVPR.2016.445.

- [13] A. Howard. "Real-time stereo visual odometry for autonomous ground vehicles." In: *2008 IEEE/RSJ International Conference on Intelligent Robots and Systems*. IEEE. 2008, pp. 1–7.
- [14] Y. Cheng, M. Maimone, and L. Matthies. "Visual odometry on the Mars Exploration Rovers." In: *2005 IEEE International Conference on Systems, Man and Cybernetics*. IEEE. 2005, pp. 1–8.
- [15] I. The MathWorks. *SLAM (Simultaneous Localization and Mapping)*. <https://de.mathworks.com/discovery/slam.html>. Accessed: 2023-08-08. 2023.
- [16] S. Vogel, H. Alkhatib, and I. Neumann. "Iterated extended Kalman filter with implicit measurement equation and nonlinear constraints for information-based georeferencing." In: *IEEE 21st International Conference on Information Fusion (FUSION)*. IEEE. 2018, pp. 1209–1216.
- [17] R. Moftizadeh, S. Vogel, I. Neumann, J. Bureick, and H. Alkhatib. "Information-Based Georeferencing of an Unmanned Aerial Vehicle by Dual State Kalman Filter with Implicit Measurement Equations." In: *Remote Sensing* 13.16 (2021), p. 3205.
- [18] L. Lucks, L. Klingbeil, L. Plümer, and Y. Dehbi. "Improving trajectory estimation using 3D city models and kinematic point clouds." In: *Transactions in GIS* 25(3) (2021).
- [19] A. Bieringer. <https://github.com/AntoniaBie/LoD3ForLocalization>. Submitted: 2023-08-22. 2023.
- [20] B. Vermessungsverwaltung. <https://geodaten.bayern.de/opengeodata>. Accessed: 2023-08-10. 2023.
- [21] J. Barbosa, B. Schwab, O. Wysocki, M. Heeramaglore, and X. Huang. <https://github.com/tum-gis/tum2twin>. Accessed: 2023-08-10. 2023.
- [22] virtualcitysystems GmbH. *VC Map*. <https://www.virtualcitymap.de>. Accessed: 2023-08-01. 2022.
- [23] OpenMMLab. <https://github.com/open-mmlab/msegmentation>. Accessed: 2023-07-20. 2023.

A. Appendix

Testing Area 1

LoD-2, real images						
Image number	Iteration	σ_x [m]	σ_y [m]	σ_z [m]	Deviation from GNSS [m]	Number of features
1 -						
2 -	15	14,72	15,51	28,74	46,30	16
3 -	10	18,39	34,89	20,62	50,75	13
4 -	25	33,16	32,99	31,09	86,54	15
5 -						
6 -						
7 -						
8 -	12	38,47	60,98	57,42	124,83	17
9 -						
10 -						
11 -						
12 -						
13 -						
14 -						
15 -						
16 -						
17 -	22	88,82	155,81	108,64	161,18	33
18 -						
19 -						
20 -						
21 -						
22 -						
23 -						
24 -						
25 -	31	112,70	37,90	78,21	172,49	19
26 -						
27 -						
28 -						
29 -						
30 -						
31 -						
32 -						
33 -						
MEDIAN:		35,81	36,39	44,25	105,69	17

LoD-2, feature images						
Image number	Iteration	σ_x [m]	σ_y [m]	σ_z [m]	Deviation from GNSS [m]	Number of features
1 -						
2 -						
3 -						
4 -						
5 -						
6 -						
7 -						
8 -						
9 -						
10 -	8	83,10	34,38	52,47	272,19	10
11 -						
12 -						
13 -						
14 -						
15 -						
16 -						
17 -						
18 -						
19 -	78	80,34	53,80	97,37	148,93	23
20 -	83	46,98	46,99	46,59	97,15	17
21 -	27	285,58	340,85	328,34	409,10	20
22 -						
23 -						
24 -						
25 -						
26 -	16	4.073,22	6.209,78	5.826,32	3.243,91	19
27 -						
28 -						
29 -						
30 -						
31 -						
32 -	27	0.72	1.54	0.3	130.02	28
33 -						
MEDIAN:		81,72	50,40	74,92	210,56	20

Testing Area 1

LoD-3, real images						
Image number	Iteration	σ_x [m]	σ_y [m]	σ_z [m]	Deviation from GNSS [m]	Number of features
1	9	13,10	20,03	15,67	38,01	23
2	-					
3	-					
4	-					
5	-					
6	18	371,83	216,41	454,72	166,08	18
7	-					
8	-					
9	-					
10	-					
11	8	13,79	32,17	18,50	68,47	24
12	-					
13	18	84,47	46,10	104,72	85,19	22
14	13	5,78	11,80	7,62	26,44	19
15	14	248,12	311,11	382,69	258,57	17
16	-					
17	15	242,64	133,88	204,92	129,85	14
18	18	15,26	52,11	21,11	53,94	14
19	-					
20	-					
21	-					
22	-					
23	-					
24	-					
25	-					
26	-					
27	-					
28	-					
29	-					
30	-					
31	-					
32	-					
33	26	1,30	1,62	0,40	107,58	13
MEDIAN:		15,26	46,10	21,11	85,19	18

LoD-3, feature images						
Image number	Iteration	σ_x [m]	σ_y [m]	σ_z [m]	Deviation from GNSS [m]	Number of features
1	-					
2	15	30,85	55,05	20,63	122,47	62
3	-					
4	-					
5	-					
6	12	99,44	152,39	127,86	243,86	53
7	12	392,44	531,17	225,84	97,61	50
8	20	24,98	105,49	31,04	119,55	54
9	-					
10	-					
11	-					
12	-					
13	23	111,87	302,08	60,18	204,84	59
14	12	149,70	495,43	124,92	406,97	45
15	-					
16	-					
17	-					
18	10	29,38	50,06	15,35	104,47	44
19	21	766,06	319,03	514,33	428,97	59
20	-					
21	-					
22	-					
23	10	19,53	62,18	21,41	110,21	53
24	-					
25	10	61,59	52,77	36,30	159,59	45
26	14	26,96	133,47	37,41	128,63	39
27	11	221,50	80,32	179,67	188,18	42
28	12	222,06	200,91	151,11	339,33	50
29	16	2.459,63	1.198,89	2.111,86	752,34	54
30	20	151,06	173,42	94,45	293,61	41
31	-					
32	-					
33	-					
MEDIAN:		111,87	152,39	94,45	188,18	50

Testing Area 1

LoD-2, sobel						
Image number	Iteration	σ_x [m]	σ_y [m]	σ_z [m]	Deviation from GNSS [m]	Number of features
1 -						
2 -						
3 -						
4 -	20	61,32	91,86	56,08	138,77	19
5 -						
6 -	67	36,60	21,86	28,81	32,85	13
7 -	15	90,81	86,32	75,62	212,88	21
8 -	17	196,43	171,97	210,23	129,09	11
9 -						
10 -						
11 -						
12 -						
13 -						
14 -						
15 -						
16 -						
17 -	15	40,61	24,91	24,62	184,20	10
18 -						
19 -						
20 -						
21 -						
22 -						
23 -	20	172,04	77,15	125,02	178,72	16
24 -	13	22,66	57,53	31,15	97,31	13
25 -						
26 -	13	70,95	36,94	82,05	188,84	15
27 -						
28 -						
29 -						
30 -						
31 -						
32 -						
33 -						
MEDIAN:		66,13	67,34	65,85	158,74	14

LoD-2, canny						
Image number	Iteration	σ_x [m]	σ_y [m]	σ_z [m]	Deviation from GNSS [m]	Number of features
1 -						
2 -						
3 -						
4 -	31	5,15	6,85	6,97	33,14	13
5 -						
6 -						
7 -	19	136,66	118,55	107,25	190,32	11
8 -						
9 -						
10 -						
11 -						
12 -						
13 -						
14 -						
15 -						
16 -						
17 -						
18 -						
19 -						
20 -	25	70,29	52,37	65,00	129,21	22
21 -						
22 -						
23 -						
24 -	9	23,14	48,17	27,40	111,12	30
25 -	24	96,04	162,22	109,41	224,70	20
26 -						
27 -						
28 -	12	27,13	41,11	39,11	110,96	26
29 -						
30 -						
31 -						
32 -						
33 -						
MEDIAN:		48,71	50,27	52,06	120,17	21

Testing Area 1

LoD-3, sobel						
Image number	Iteration	σ_x [m]	σ_y [m]	σ_z [m]	Deviation from GNSS [m]	Number of features
1 -						
2 -						
3 -	47	51,23	49,85	24,65	76,74	13
4 -						
5 -						
6 -						
7 -	14	232,81	67,45	132,66	155,55	19
8 -	10	106,91	167,19	158,37	106,66	6
9 -	14	23,23	25,07	17,73	52,94	10
10 -	11	404,45	588,15	447,58	234,45	12
11 -	7	347,75	141,17	49,17	450,33	6
12 -	12	36,59	44,46		74,36	17
13 -		54,04				
14 -						
15 -	18	28,79	30,15	15,58	62,16	15
16 -	13	3,34	11,73	1,46	43,76	13
17 -						
18 -						
19 -						
20 -	12	686,24	399,70	477,92	266,96	7
21 -	8	43,25	67,27	31,64	63,28	15
22 -						
23 -						
24 -						
25 -						
26 -						
27 -						
28 -						
29 -						
30 -	13	6,37	13,65	6,98	29,29	16
31 -						
32 -						
33 -						
MEDIAN:		51,23	58,56	31,64	75,55	13

LoD-3, canny						
Image number	Iteration	σ_x [m]	σ_y [m]	σ_z [m]	Deviation from GNSS [m]	Number of features
1 -	29	2,24	5,72	1,67	57,84	18
2 -						
3 -						
4 -						
5 -						
6 -						
7 -	163	37,67	127,13	77,54	153,05	14
8 -						
9 -	9	57,38	44,44	51,99	102,74	17
10 -	10	124,09	132,50	116,25	120,05	25
11 -						
12 -	9	33,98	49,92	22,30	88,25	24
13 -						
14 -	13	137,12	210,40	213,87	237,83	23
15 -						
16 -						
17 -						
18 -						
19 -						
20 -						
21 -						
22 -						
23 -	9	47,11	93,58	32,33	174,05	16
24 -						
25 -	89	0,76	0,95	0,54	104,56	31
26 -						
27 -	10	18,58	10,47	15,41	35,38	20
28 -	14	33,45	16,87	16,93	38,13	21
29 -						
30 -						
31 -						
32 -						
33 -						
MEDIAN:		35,82	47,18	27,31	103,65	21

Testing Area 1

LoD-2, mask						
Image number	Iteration	σ_x [m]	σ_y [m]	σ_z [m]	Deviation from GNSS [m]	Number of features
1 -						
2 -	34	88,32	78,90	92,22	123,75	17
3 -						
4 -						
5 -	14	13,85	20,55	15,79	39,31	24
6 -						
7 -						
8 -						
9 -						
10 -						
11 -						
12 -						
13 -						
14 -						
15 -						
16 -						
17 -						
18 -						
19 -						
20 -	17	25,01	25,97	34,99	156,73	19
21 -						
22 -						
23 -						
24 -						
25 -	13	14,85	38,68	23,30	87,19	17
26 -						
27 -						
28 -						
29 -						
30 -						
31 -						
32 -						
33 -						
MEDIAN:		19,93	32,32	29,15	105,47	18

LoD-2, mask and sobel						
Image number	Iteration	σ_x [m]	σ_y [m]	σ_z [m]	Deviation from GNSS [m]	Number of features
1 -						
2 -	17	22,61	18,80	25,85	100,91	14
3 -						
4 -						
5 -	10	58,44	73,24	74,64098032	102,41	21
6 -						
7 -	9	53,49	74,99	59,12	213,95	22
8 -						
9 -						
10 -						
11 -						
12 -						
13 -						
14 -						
15 -						
16 -						
17 -						
18 -	11	25,35	34,10	28,58	100,51	21
19 -						
20 -	21	7,32	10,43	8,48	81,86	17
21 -						
22 -						
23 -						
24 -	16	106,65	109,45	123,00	154,84	17
25 -	21	116,44	101,58	147,13	166,74	26
26 -						
27 -	25	66,54	111,17	68,70	111,49	22
28 -						
29 -						
30 -						
31 -						
32 -						
33 -						
MEDIAN:		55,96	74,12	59,12	106,95	21

Testing Area 1

LoD-3, mask						
Image number	Iteration	σ_x [m]	σ_y [m]	σ_z [m]	Deviation from GNSS [m]	Number of features
1	21	1,39	1,52	0,60	18,52	19
2						
3						
4						
5						
6						
7						
8						
9						
10						
11	16	2,29	6,17	2,73	90,58	12
12						
13						
14						
15						
16	25	12662,43	6784,07	7057,78	1567,45	18
17						
18	13	56,26	44,57	48,74	110,42	18
19						
20	19	173,86	185,68	50,68	156,33	14
21						
22						
23						
24						
25						
26						
27						
28						
29						
30						
31						
32						
33						
MEDIAN:		56,26	44,57	48,74	110,42	18

LoD-3, mask and sobel						
Image number	Iteration	σ_x [m]	σ_y [m]	σ_z [m]	Deviation from GNSS [m]	Number of features
1						
2						
3						
4						
5						
6						
7						
8						
9						
10	10	102,73	70,82	70,48	127,76	8
11						
12						
13	23	491,93	1141,56	957,19	300,41	10
14						
15						
16	12	12,70	13,05	10,92	46,30	10
17	50	130,62	29,03	74,98	46,28	12
18						
19						
20						
21						
22	9	12,75	15,20	9,23	28,10	17
23						
24						
25						
26						
27						
28						
29						
30						
31						
32	26	28,84	17,82	13,97	18,41	16
33						
MEDIAN:		65,78	23,43	42,22	46,29	11

Testing Area 1

LoD-2, mask and canny						
Image number	Iteration	σ_x [m]	σ_y [m]	σ_z [m]	Deviation from GNSS [m]	Number of features
1 -						
2 -						
3 -						
4 -						
5 -						
6 -	21	53,60	34,64	50,31	129,40	45
7 -						
8 -						
9 -						
10 -						
11 -						
12 -						
13 -						
14 -						
15 -						
16 -						
17 -						
18 -	12	59,45	92,93	42,70	86,85	34
19 -						
20 -						
21 -						
22 -						
23 -	14	92,25	135,74	95,42	146,37	26
24 -						
25 -						
26 -						
27 -						
28 -						
29 -						
30 -						
31 -						
32 -						
33 -						
MEDIAN:		59,45	92,93	50,31	129,40	34

Testing Area 1

LoD-3, mask and canny						
Image number	Iteration	σ_x [m]	σ_y [m]	σ_z [m]	Deviation from GNSS [m]	Number of features
1	16	20,67	12,80	7,16	92,44	12
2	-					
3	13	84,50	116,81	109,08	91,67	14
4	36	2,56	5,02	1,04	58,14	25
5	-					
6	-					
7	10	99,42	148,39	155,10	201,99	27
8	-					
9	13	272,06	822,69	181,01	366,32	22
10	11	1497,06	628,53	1454,84	498,95	28
11	9	38,27	77,70	42,67	98,44	18
12	8	8,94	20,20	10,51	49,56	24
13	27	18,81	55,16	19,57	91,62	31
14	-					
15	12	7,00	16,33	8,00	52,65	22
16	-					
17	-					
18	24	51,75	117,46	80,90	190,28	27
19	-					
20	-					
21	-					
22	-					
23	-					
24	11	24,01	55,16	18,75	98,08	19
25	113	1.640,71	887,48	1.797,85	514,21	21
26	-					
27	-					
28	-					
29	16	11,62	20,77	13,07	95,15	17
30	-					
31	-					
32	-					
33	10	87,49	46,46	63,66	167,75	12
MEDIAN:		38,27	55,16	42,67	98,08	22

Testing Area 2

LoD-2, real images						
Image number	Iteration	σ_x [m]	σ_y [m]	σ_z [m]	Deviation from GNSS [m]	Number of features
1 -						
2 -	20	230,69	168,56	243,04	198,08	8
3 -						
4 -	13	105,43	91,76	107,97	151,79	14
5 -	9	25,70	42,25	37,35	62,37	12
6 -						
7 -	13	30,98	19,80	22,59	100,68	14
8 -	40	48,02	44,22	58,98	165,89	10
9 -						
10 -						
11 -						
12 -						
13 -						
14 -						
15 -						
16 -						
17 -						
18 -						
19 -						
20 -						
21 -						
22 -						
23 -						
24 -						
25 -						
26 -						
27 -						
28 -						
29 -						
30 -						
31 -						
32 -						
33 -						
34 -						
35 -						
36 -						
37 -						
38 -						
39 -						
40 -						
41 -						
42 -						
43 -						
44 -						
45 -						
46 -						
47 -						
48 -						
49 -						
MEDIAN:		48,02	44,22	58,98	151,79	12

Testing Area 2

LoD-3, real images						
Image number	Iteration	σ_x [m]	σ_y [m]	σ_z [m]	Deviation from GNSS [m]	Number of features
1	-					
2	-					
3	15	10,55	41,67	15,48	127,41	10
4	-					
5	-					
6	-					
7	20	17,49	41,38	17,08	259,01	10
8	-					
9	51	0,03	0,07	0,04	141,95	9
10	-					
11	-					
12	14	81,99	26,31	49,33	124,22	14
13	20	51,70	77,16	67,46	75,35	9
14	-					
15	-					
16	-					
17	-					
18	-					
19	-					
20	-					
21	-					
22	-					
23	-					
24	-					
25	-					
26	10	128,77	140,87	214,03	194,05	6
27	18	14,43	76,54	96,02	458,17	6
28	-					
29	-					
30	-					
31	-					
32	-					
33	-					
34	-					
35	-					
36	-					
37	-					
38	-					
39	-					
40	-					
41	-					
42	-					
43	-					
44	-					
45	-					
46	-					
47	-					
48	-					
49	-					
MEDIAN:		17,49	41,67	49,33	141,95	9

Testing Area 2

LoD-2, feature images						
Image number	Iteration	σ_x [m]	σ_y [m]	σ_z [m]	Deviation from GNSS [m]	Number of features
1	-					
2	-					
3	15	188,57	536,52	260,16	480,02	29
4	54	237,45	723,65	350,08	805,62	17
5	-					
6	41	32,52	62,81	27,90	123,59	20
7	33	1706,49	1075,50	1490,89	1145,99	30
8	-					
9	-					
10	-					
11	-					
12	-					
13	32	14,15	7,20	3,96	24,82	28
14	-					
15	12	130,94	224,72	201,62	321,76	31
16	18	788,15	986,73	874,06	590,69	18
17	-					
18	-					
19	25	222,60	174,47	194,87	536,59	24
20	-					
21	-					
22	24	1.331,22	903,73	1.296,17	726,65	35
23	13	49,22	22,81	17,83	65,10	19
24	17	126,04	118,36	94,34	205,25	32
25	-					
26	16	47,70	32,42	35,76	231,61	29
27	-					
28	23	44,85	191,27	80,88	141,08	20
29	-					
30	-					
31	-					
32	21	3.516,54	2.612,72	2.835,70	1866,56	16
33	-					
34	-					
35	-					
36	-					
37	-					
38	-					
39	-					
40	22	26,84	13,53	18,02	312,10	10
41	-					
42	-					
43	-					
44	-					
45	-					
46	-					
47	-					
48	11	258,04	470,94	395,47	436,87	8
49	12	70,59	101,10	108,25	129,49	7
MEDIAN:		130,94	191,27	194,87	321,76	20

Testing Area 2

LoD-3, feature images						
Image number	Iteration	σ_x [m]	σ_y [m]	σ_z [m]	Deviation from GNSS [m]	Number of features
1	-					
2	16	28,37	37,47	15,21	73,40	55
3	11	77,02	16,88	29,51	119,57	61
4	-					
5	12	168,78	118,17	75,17	110,17	50
6	17	284,59	214,84	235,73	239,67	64
7	-					
8	-					
9	10	48,73	85,65	70,51	66,71	63
10	12	241,84	266,38	279,67	438,99	81
11	9	43,29	64,76	43,91	56,78	62
12	-					
13	12	376,91	620,67	373,58	340,23	89
14	17	252,76	384,60	279,52	259,35	79
15	10	77,42	35,17	48,41	111,93	91
16	16	36,76	55,51	21,85	258,69	39
17	11	115,6484	334,8245	158,2168	201,3318	68
18	-					
19	23	319,75	169,88	280,64	229,25	31
20	-					
21	-					
22	13	673,10	1.399,39	975,60	459,37	50
23	11	33,12	63,17	41,55	80,85	45
24	-					
25	10	40,83	65,80	31,13	80,17	66
26	13	25,83	44,98	22,11	89,24	86
27	27	900,38	487,82	1.139,89	695,35	74
28	15	280,66	245,93	279,62	534,51	87
29	14	231,10	234,59	281,86	559,06	65
30	-					
31	13	364,33	503,18	407,70	916,85	83
32	-					
33	-					
34	-					
35	-					
36	-					
37	-					
38	-					
39	-					
40	-					
41	-					
42	-					
43	-					
44	-					
45	-					
46	-					
47	-					
48	-					
49	-					
MEDIAN:		168,78	169,88	158,22	229,25	65

Testing Area 2

LoD-2, sobel						
Image number	Iteration	σ_x [m]	σ_y [m]	σ_z [m]	Deviation from GNSS[m]	Number of features
1 -						
2 -						
3 -						
4 -						
5 -						
6 -						
7	35	243,97	172,83	253,28	171,64	10
8	17	157,84	146,98	164,46	164,26	7
9 -						
10	16	39,31	64,62	48,69	134,81	9
11 -						
12	9	43,37	49,84	51,87	45,45	10
13	26	52,51	33,71	20,53	122,19	6
14 -						
15 -						
16 -						
17 -						
18 -						
19 -						
20	27	466,78	184,26	258,89	249,28	13
21 -						
22 -						
23 -						
24	24	93,47	76,02	7,98	139,46	11
25 -						
26 -						
27 -						
28 -						
29 -						
30 -						
31 -						
32 -						
33 -						
34 -						
35 -						
36 -						
37 -						
38 -						
39 -						
40 -						
41 -						
42 -						
43 -						
44 -						
45 -						
46 -						
47 -						
48 -						
49 -						
MEDIAN:		93,47	76,02	51,87	139,46	10

Testing Area 2

LoD-3, sobel						
Image number	Iteration	σ_x [m]	σ_y [m]	σ_z [m]	Deviation from GNSS [m]	Number of features
1	-					
2	16	44,42	29,95	22,76	127,74	10
3	-					
4	10	15,42	28,37	3,01	119,45	7
5	-					
6	-					
7	-					
8	-					
9	16	48,74	55,70	29,25	75,09	11
10	-					
11	-					
12	11	47,78	24,71	69,42	111,97	10
13	-					6
14	-					
15	-					
16	10	25,64	13,95	16,04	152,12	5
17	-					
18	11	18,28	28,97	15,74	118,14	7
19	-					
20	-					
21	-					
22	-					
23	-					
24	-					
25	-					
26	-					
27	-					
28	-					
29	20	4,37	13,77	4,69	63,49	10
30	-					
31	20	1,63	3,65	1,38	128,30	10
32	-					
33	-					
34	-					
35	-					
36	-					
37	-					
38	-					
39	-					
40	-					
41	-					
42	-					
43	-					
44	-					
45	-					
46	-					
47	-					
48	-					
49	-					
MEDIAN:		21,96	26,54	15,89	118,80	10

Testing Area 2

LoD-2, canny						
Image number	Iteration	σ_x [m]	σ_y [m]	σ_z [m]	Deviation from GNSS [m]	Number of features
1	-					
2	-					
3	-					
4	-					
5	42	21,80	24,39	16,63	303,15	9
6	11	8,51	12,97	8,82	26,80	18
7	-					
8	-					
9	18	71,57	51,04	45,37	67,33	8
10	-					
11	-					
12	-					
13	-					
14	27	67,40	83,78	42,97	45,32	8
15	-					
16	-					
17	-					
18	-					
19	-					
20	-					
21	-					
22	-					
23	-					
24	-					
25	-					
26	-					
27	-					
28	-					
29	29	159,67	236,16	349,67	133,99	12
30	-					
31	-					
32	-					
33	-					
34	-					
35	-					
36	-					
37	-					
38	-					
39	-					
40	-					
41	-					
42	-					
43	-					
44	-					
45	-					
46	17	39,77	15,19	14,70	289,08	6
47	-					
48	-					
49	31	43,62	20,26	38,84	344,01	8
MEDIAN:		43,62	24,39	38,84	133,99	8

Testing Area 2

LoD-3, canny						
Image number	Iteration	σ_x [m]	σ_y [m]	σ_z [m]	Deviation from GNSS [m]	Number of features
1	-					
2	9	174,41	89,85	175,02	116,72	14
3	-					
4	-					
5	13	53,27	36,86	56,27	93,48	8
6	-					
7	-					
8	21	22,77	38,64	14,74	265,25	15
9	-					
10	18	21,27	51,77	16,75	48,46	16
11	17	22,36	52,87	17,15	57,53	15
12	25	48,33	81,94	33,06	66,50	13
13	-					
14	-					
15	-					
16	-					
17	-					
18	-					
19	-					
20	-					
21	-					
22	-					
23	-					
24	-					
25	-					
26	-					
27	-					
28	-					
29	-					
30	-					
31	-					
32	-					
33	-					
34	-					
35	21	52,84	87,15	62,42	44,66	6
36	-					
37	-					
38	-					
39	-					
40	-					
41	-					
42	-					
43	-					
44	-					
45	-					
46	-					
47	-					
48	-					
49	-					
MEDIAN:		48,33	52,87	33,06	66,50	14

Testing Area 2

LoD-2, mask						
Image number	Iteration	σ_x [m]	σ_y [m]	σ_z [m]	Deviation from GNSS [m]	Number of features
1 -						
2 -	22	3,19	10,52	2,39	37,51	13
3 -						
4 -						
5 -						
6 -	12	121,47	216,08	142,48	162,66	22
7 -						
8 -	14	640,65	510,04	634,77	361,53	21
9 -						
10 -						
11 -						
12 -						
13 -	66	6,08	10,10	2,66	199,14	14
14 -						
15 -	8	13,16	13,27	21,57	34,87	16
16 -						
17 -						
18 -						
19 -	16	2,06	13,92	7,70	108,41	8
20 -						
21 -						
22 -						
23 -						
24 -						
25 -						
26 -						
27 -						
28 -						
29 -						
30 -						
31 -						
32 -						
33 -						
34 -						
35 -						
36 -						
37 -						
38 -						
39 -						
40 -						
41 -						
42 -						
43 -						
44 -						
45 -						
46 -						
47 -						
48 -						
49 -						
MEDIAN:		9,62	13,59	14,63	135,54	15

Testing Area 2

LoD-3, mask						
Image number	Iteration	σ_x [m]	σ_y [m]	σ_z [m]	Deviation from GNSS [m]	Number of features
1	11	13,77	25,69	13,18	133,89	15
2	-					
3	-					
4	-					
5	-					
6	-					
7	-					
8	-					
9	-					
10	-					
11	-					
12	-					
13	-					
14	-					
15	13	8,72	43,75	8,02	62,52	22
16	-					
17	-					
18	-					
19	-					
20	-					
21	-					
22	27	10,79	10,98	10,12	54,67	10
23	-					
24	-					
25	-					
26	-					
27	-					
28	11	36,23	9,81	2,59	215,14	6
29	10	74,41	35,70	46,26	87,13	12
30	-					
31	-					
32	-					
33	-					
34	-					
35	-					
36	-					
37	-					
38	-					
39	-					
40	-					
41	-					
42	-					
43	-					
44	-					
45	-					
46	-					
47	-					
48	-					
49	-					
MEDIAN:		13,77	25,69	10,12	87,13	12

Testing Area 2

LoD-2, mask and sobel						
Image number	Iteration	σ_x [m]	σ_y [m]	σ_z [m]	Deviation from GNSS [m]	Number of features
1	-					
2	-					
3	30	160,78	164,78	166,24	309,92	26
4	11	40,50	41,14	27,14	95,34	25
5	10	110,55	118,56	85,69	223,65	24
6	-					
7	-					
8	-					
9	-					
10	-					
11	18	224,19	221,62	246,42	126,72	12
12	60	67,45	91,99	110,48	181,12	13
13	13	328,71	171,79	324,93	286,80	15
14	78	50,16	40,43	35,84	43,71	9
15	138	85,06	150,24	119,09	153,11	18
16	-					
17	-					
18	-					
19	15	0,32	1,04	0,45	17,44	13
20	-					
21	10	53,15	70,52	96,01	67,21	10
22	9	3,52	4,85	3,41	36,70	13
23	26	169,69	396,84	498,96	145,59	13
24	-					
25	-					
26	-					
27	21	27,64	67,78	20,15	46,43	8
28	-					
29	-					
30	-					
31	-					
32	-					
33	-					
34	-					
35	-					
36	-					
37	-					
38	-					
39	-					
40	-					
41	-					
42	-					
43	-					
44	-					
45	-					
46	-					
47	-					
48	-					
49	-					
MEDIAN:		67,45	91,99	96,01	126,72	13

Testing Area 2

LoD-3, mask and sobel						
Image number	Iteration	σ_x [m]	σ_y [m]	σ_z [m]	Deviation from GNSS [m]	Number of features
1	-					
2	13	37,77	81,32	46,71	75,01	9
3	-					
4	18	227,91	378,69	142,77	79,58	14
5	-					
6	16	44,01	38,25	6,87	101,28	11
7	14	40,58	23,86	36,39	250,18	15
8	-					
9	18	876,23	580,95	358,40	227,27	17
10	-					
11	-					
12	-					
13	-					
14	-					
15	-					
16	9	582,67	521,82	677,85	109,74	10
17	-					
18	6	29,35	73,08	50,09	55,13	10
19	13	40,19	85,56	65,05	59,01	11
20	26	161,43	110,06	176,01	160,26	16
21	8	94,36	66,45	80,71	40,78	16
22	10	231,87	127,70	120,50	141,74	15
23	-					
24	-					
25	-					
26	-					
27	-					
28	-					
29	-					
30	-					
31	-					
32	-					
33	-					
34	-					
35	-					
36	-					
37	-					
38	-					
39	-					
40	-					
41	-					
42	-					
43	-					
44	-					
45	-					
46	-					
47	-					
48	-					
49	-					
MEDIAN:		94,36	85,56	80,71	101,28	14

Testing Area 2

LoD-2, mask and canny						
Image number	Iteration	σ_x [m]	σ_y [m]	σ_z [m]	Deviation from GNSS [m]	Number of features
1	14	337,44	212,95	309,41	310,37	20
2	10	233,32	319,68	207,93	339,29	22
3	13	40,74	96,67	46,24	162,59	39
4	13	80,94	100,80	125,44	172,60	39
5	-					
6	-					
7	12	40,72	52,83	47,77	104,54	39
8	8	219,25	149,61	218,53	213,53	27
9	16	44,79	62,26	59,64	100,82	23
10	12	18,30	13,26	6,60	50,15	21
11	6	48,68	29,00	40,02	70,53	20
12	-					
13	-					
14	-					
15	-					
16	-					
17	-					
18	-					
19	24	34,77	81,45	41,36	167,26	11
20	-					
21	-					
22	-					
23	-					
24	-					
25	-					
26	153	5,49	11,66	8,10	27,21	16
27	-					
28	-					
29	-					
30	-					
31	-					
32	-					
33	12	0,42	1,05	0,15	277,01	17
34	-					
35	-					
36	-					
37	-					
38	15	11,26	17,82	7,44	192,92	27
39	-					
40	-					
41	-					
42	-					
43	13	26,51	22,46	19,92	211,35	11
44	16	8,10	6,43	11,54	204,54	10
45	-					
46	16	34,02	23,86	34,11	171,19	16
47	-					
48	-					
49	-					
MEDIAN:		37,74	40,91	40,69	171,89	21

Testing Area 2

LoD-3, mask and canny						
Image number	Iteration	σ_x [m]	σ_y [m]	σ_z [m]	Deviation from GNSS [m]	Number of features
1	14	27,01	49,74	19,65	93,15	39
2	-					
3	10	54,27	134,33	59,24	17,14	29
4	-					
5	-					
6	-					
7	8	36,04	57,63	24,60	64,43	30
8	8	63,70	43,19	22,24	90,97	39
9	8	35,16	41,96	13,88	72,27	38
10	-					
11	-					
12	18	241,33	142,97	294,39	293,09	27
13	-					
14	-					
15	12	0,54	0,46	0,23	88,00	23
16	-					
17	6	42,08	58,02	42,56	67,95	11
18	17	81,39	80,06	102,49	58,24	11
19	10	68,28	108,23	94,97	75,36	15
20	-					
21	-					
22	-					
23	-					
24	-					
25	-					
26	-					
27	-					
28	-					
29	-					
30	-					
31	-					
32	-					
33	10	62,86	296,30	126,12	175,83	12
34	-					
35	-					
36	-					
37	-					
38	-					
39	-					
40	-					
41	-					
42	-					
43	-					
44	-					
45	24	1,53	6,85	0,77	104,56	29
46	-					
47	-					
48	63	40,33	122,98	27,19	205,55	15
49	-					
MEDIAN:		42,08	58,02	27,19	88,00	27

Testing Area 3

LoD-2, real images							
Image number	Iteration	σ_x [m]	σ_y [m]	σ_z [m]	Deviation from GNSS [m]	Number of features	
1	-						
2	21	43,54	67,55	76,92	178,19		12
3	-						
4	-						
5	27	71,12	132,48	99,08	245,67		28
6	-						
7	-						
8	33	36,27	28,03	32,62	148,41		18
9	-						
10	-						
11	38	99,10	84,91	109,77	157,70		20
12	-						
13	-						
14	-						
15	-						
16	-						
17	14	123,04	99,22	79,35	52,84		9
18	9	71,62	49,34	81,17	142,32		9
19	-						
20	-						
21	-						
22	-						
23	-						
24	-						
25	-						
26	-						
27	-						
28	-						
29	-						
30	-						
31	-						
32	-						
MEDIAN:		71,37	76,23	80,26	153,05		15

LoD-2, feature images							
Image number	Iteration	σ_x [m]	σ_y [m]	σ_z [m]	Deviation from GNSS [m]	Number of features	
1	-						
2	-						
3	-						
4	-						
5	-						
6	-						
7	-						
8	-						
9	-						
10	-						
11	98	128,83	65,59	40,43	146,48		25
12	32	35,64	19,11	6,07	153,24		20
13	14	18,43	16,51	11,17	35,80		20
14	21	242,95	137,08	47,15	581,00		23
15	-						
16	-						
17	-						
18	-						
19	-						
20	-						
21	27	133,86	65,78	29,54	152,82		19
22	17	95,35	348,96	161,08	291,81		18
23	-						
24	17	277,85	419,88	290,95	594,80		14
25	30	2.461,76	972,98	2.138,98	1.267,82		25
26	-						
27	24	522,72	469,01	431,36	953,75		21
28	11	208,17	118,31	173,20	366,70		20
29	-						
30	-						
31	-						
32	-						
MEDIAN:		171,01	127,70	104,11	329,25		20

Testing Area 3

LoD-3, real images						
Image number	Iteration	σ_x [m]	σ_y [m]	σ_z [m]	Deviation from GNSS [m]	Number of features
1 -						
2 -						
3 -						
4 -						
5 -						
6 -						
7 -						
8 -						
9 -	21	15,46	48,94	19,66	120,30	26
10 -						
11 -						
12 -						
13 -						
14 -						
15 -	15	94,54	83,52	134,76	135,82	34
16 -	46	64,64	276,51	143,53	355,27	10
17 -						
18 -	35	0,12	0,36	0,08	221,69	9
19 -						
20 -						
21 -						
22 -						
23 -						
24 -						
25 -						
26 -						
27 -						
28 -						
29 -						
30 -						
31 -						
32 -						
MEDIAN:		40,05	66,23	77,21	178,76	18

LoD-3, feature images						
Image number	Iteration	σ_x [m]	σ_y [m]	σ_z [m]	Deviation from GNSS [m]	Number of features
1 -						
2 -	12	46,59	101,85	36,72	102,46	56
3 -						
4 -						
5 -						
6 -	14	88,65	70,88	95,97	100,09	62
7 -	11	38,22	74,97	30,10	79,76	40
8 -						
9 -						
10 -	10	29,89	81,19	31,21	101,01	47
11 -						
12 -						
13 -	17	19,47	65,81	21,44	185,12	42
14 -						
15 -						
16 -						
17 -	27	68,86	46,34	39,25	358,40	61
18 -						
19 -						
20 -	13	21,14	38,17	9,99	129,06	52
21 -	31	152,59	18,95	88,22	121,83	56
22 -						
23 -	17	8,66	20,45	4,21	269,79	52
24 -						
25 -						
26 -						
27 -						
28 -	29	3,62	4,96	2,23	169,13	38
29 -	41	1,56	5,51	0,76	224,17	33
30 -	64	0,16	0,28	0,06	208,90	39
31 -						
32 -	12	12,26	33,25	12,40	279,10	34
MEDIAN:		21,14	38,17	21,44	169,13	47

Testing Area 3

LoD-2, sobel						
Image number	Iteration	σ_x [m]	σ_y [m]	σ_z [m]	Deviation from GNSS [m]	Number of features
1 -						
2 -						
3 -						
4 -						
5 -						
6 -						
7	10	124,76	57,19	101,05	107,96	12
8	24	76,53	61,82	116,45	100,13	16
9 -						
10 -						
11	26	61,92	21,87	34,32	39,59	13
12	14	330,56	192,51	471,04	185,72	14
13	19	57,64	29,88	51,03	59,52	15
14 -						
15 -						
16	14	28,19	24,89	20,10	81,00	7
17	19	30,09	24,84	31,70	62,99	6
18 -						
19	23	54,44	66,49	30,84	47,69	9
20 -						
21 -						
22 -						
23 -						
24 -						
25 -						
26 -						
27 -						
28 -						
29 -						
30 -						
31 -						
32 -						
MEDIAN:		59,78	43,54	42,67	72,00	13

LoD-2, canny						
Image number	Iteration	σ_x [m]	σ_y [m]	σ_z [m]	Deviation from GNSS [m]	Number of features
1 -						
2 -						
3 -						
4 -						
5 -						
6 -						
7 -						
8 -						
9	8	25,42	31,44	19,74	89,53	17
10 -						
11 -						
12 -						
13 -						
14	16	38,66	35,18	34,32	57,52	15
15	20	22,14	61,42	35,57	53,09	10
16 -						
17	22	20,33	18,61	18,51	70,26	16
18	13	104,20	65,20	17,86	126,51	12
19 -						
20 -						
21	11	24,55	20,31	5,77	64,98	11
22 -						
23 -						
24 -						
25 -						
26 -						
27 -						
28 -						
29 -						
30 -						
31 -						
32 -						
MEDIAN:		24,98	33,31	19,12	67,62	14

Testing Area 3

LoD-3, sobel						
Image number	Iteration	σ_x [m]	σ_y [m]	σ_z [m]	Deviation from GNSS [m]	Number of features
1 -						
2 -						
3 -						
4 -						
5 -						
6 -						
7 -						
8 -						
9 -	12	53,26	86,82	51,06	110,79	14
10 -	125	0,01	0,03	0,00	220,06	15
11 -						
12 -						
13 -	19	94,93	94,23	80,89	122,04	17
14 -	14	28,17	44,79	19,09	317,26	14
15 -						
16 -						
17 -						
18 -						
19 -						
20 -						
21 -						
22 -						
23 -						
24 -						
25 -						
26 -						
27 -						
28 -						
29 -						
30 -						
31 -						
32 -						
MEDIAN:		40,71	65,81	35,07	171,05	15

LoD-3, canny						
Image number	Iteration	σ_x [m]	σ_y [m]	σ_z [m]	Deviation from GNSS [m]	Number of features
1 -						
2 -	53	1,94	3,43	1,00	221,61	21
3 -	12	17,85	59,25	26,09	194,41	27
4 -	92	1,71	4,35	1,20	233,54	21
5 -						
6 -						
7 -	13	223,22	139,21	314,55	166,64	19
8 -						
9 -						
10 -						
11 -						
12 -						
13 -	22	16,56	41,55	22,21	138,91	22
14 -						
15 -	41	0,19	0,21	0,05	193,53	12
16 -						
17 -						
18 -	17	27,13	18,88	10,94	154,36	14
19 -						
20 -	30	2,13	3,22	1,09	227,36	12
21 -						
22 -						
23 -						
24 -						
25 -						
26 -						
27 -						
28 -						
29 -						
30 -						
31 -						
32 -						
		9,35	11,62	6,07	193,97	20

Testing Area 3

LoD-2, mask						
Image number	Iteration	σ_x [m]	σ_y [m]	σ_z [m]	Deviation from GNSS [m]	Number of features
1 -						
2 -						
3 -						
4 -						
5 -						
6 -						
7 -						
8 -	13	43,62	23,25	23,58	81,28	17
9 -						
10 -						
11 -						
12 -	22	22,20	13,61	14,82	38,71	12
13 -	14	34,19	43,76	56,70	39,61	13
14 -	12	234,44	283,51	349,68	668,84	11
15 -						
16 -						
17 -						
18 -						
19 -						
20 -						
21 -						
22 -						
23 -						
24 -						
25 -						
26 -						
27 -						
28 -						
29 -						
30 -						
31 -						
32 -						
MEDIAN:		38,90	33,51	40,14	60,44	13

LoD-2, mask and sobel						
Image number	Iteration	σ_x [m]	σ_y [m]	σ_z [m]	Deviation from GNSS [m]	Number of features
1 -						
2 -	25	19,34	23,25	19,21	105,12	18
3 -						
4 -						
5 -	771	4,10	3,18	2,48	67,71	12
6 -	18	200,62	109,52	100,58	132,80	19
7 -						
8 -						
9 -	17	14,55	11,16	9,14	27,29	15
10 -						
11 -						
12 -						
13 -						
14 -						
15 -	21	101,14	69,23	83,20	93,67	12
16 -						
17 -						
18 -						
19 -						
20 -						
21 -	9	21,05	20,30	12,04	57,82	16
22 -						
23 -						
24 -						
25 -	35	307,37	150,11	276,09	116,44	10
26 -						
27 -						
28 -						
29 -						
30 -						
31 -						
32 -						
MEDIAN:		21,05	23,25	19,21	93,67	15

Testing Area 3

LoD-3, mask						
Image number	Iteration	σ_x [m]	σ_y [m]	σ_z [m]	Deviation from GNSS [m]	Number of features
1	-					
2	-					
3	16	98,42	222,01	151,61	127,33	10
4	-					
5	14	63,13	107,62	86,83	152,17	30
6	24	19,16	43,32	15,81	303,36	23
7	-					
8	15	627,77	683,10	709,41	297,66	27
9	-					
10	109	1,84	4,18	1,12	211,46	22
11	-					
12	-					
13	17	21,03	77,36	40,13	270,42	18
14	35	2,98	5,80	0,42	219,85	14
15	14	15,68	18,79	11,46	138,75	15
16	-					
17	-					
18	-					
19	-					
20	-					
21	-					
22	-					
23	-					
24	-					
25	-					
26	-					
27	-					
28	-					
29	-					
30	-					
31	-					
32	-					
MEDIAN:		20,10	60,34	27,97	215,65	20

LoD-3, mask and sobel						
Image number	Iteration	σ_x [m]	σ_y [m]	σ_z [m]	Deviation from GNSS [m]	Number of features
1	27	0,07	0,12	0,02	246,02	19
2	-					
3	-					
4	-					
5	19	68,51	88,62	71,43	332,21	19
6	22	32,36	51,77	43,16	127,43	25
7	-					
8	-					
9	-					
10	32	90,43	73,18	74,16	76,24	16
11	20	34,87	77,74	46,81	322,35	17
12	-					
13	81	2,59	6,63	0,87	237,11	11
14	-					
15	-					
16	24	28,93	15,44	15,37	241,01	16
17	-					
18	-					
19	-					
20	-					
21	-					
22	-					
23	-					
24	15	59,29	43,99	68,04	172,81	11
25	-					
26	-					
27	-					
28	-					
29	-					
30	-					
31	-					
32	-					
MEDIAN:		33,62	47,88	44,98	239,06	17

Testing Area 3

LoD-2, mask and canny						
Image number	Iteration	σ_x [m]	σ_y [m]	σ_z [m]	Deviation from GNSS [m]	Number of features
1	-					
2	21	207,71	164,95	214,44	268,24	26
3	-					
4	-					
5	-					
6	-					
7	-					
8	40	742,30	836,54	878,37	459,68	32
9	-					
10	19	151,14	109,19	168,30	173,29	28
11	37	259,00	242,17	282,77	344,44	26
12	-					
13	-					
14	36	159,73	176,43	180,55	214,45	25
15	335	24,73	41,32	24,23	110,46	27
16	-					
17	-					
18	-					
19	-					
20	-					
21	-					
22	-					
23	-					
24	-					
25	11	153,48	168,19	95,11	98,34	7
26	-					
27	-					
28	-					
29	-					
30	-					
31	-					
32	-					
MEDIAN:		159,73	168,19	180,55	214,45	26

Testing Area 3

LoD-3, mask and canny						
Image number	Iteration	σ_x [m]	σ_y [m]	σ_z [m]	Deviation from GNSS [m]	Number of features
1 -						
2 -						
3 -	16	7,83	13,24	5,19	195,31	28
4 -						
5 -						
6 -						
7 -						
8 -						
9 -						
10 -						
11 -						
12 -	35	0,02	0,03	0,02	197,78	28
13 -	28	0,43	1,48	0,37	242,12	25
14 -						
15 -	47	112,16	91,23	131,08	98,97	21
16 -						
17 -	34	0,76	0,56	0,30	178,08	14
18 -						
19 -	45	24,79	18,02	22,36	131,67	16
20 -						
21 -	21	132,31	59,37	117,23	183,57	12
22 -						
23 -						
24 -						
25 -						
26 -						
27 -						
28 -						
29 -						
30 -						
31 -						
32 -						
MEDIAN:		7,83	13,24	5,19	183,57	21